# QUANTITATIVE CHARACTERIZATION TECHNOLOGY FOR NANOMETER SPACED HEAD-DISK SYSTEMS

JIANG YING

NATIONAL UNIVERSITY OF SINGAPORE

2004

# QUANTITATIVE CHARACTERIZATION TECHNOLOGY FOR NANOMETER SPACED HEAD-DISK SYSTEMS

**JIANG YING**

**A THESIS SUBMITTED**
**FOR THE DEGREE OF MASTER OF ENGINEERING**
**DEPARTMENT OF ELECTRICAL AND COMPUTER ENGINEERING**
**NATIONAL UNIVERSITY OF SINGAPORE**
**2004**

# Acknowledgements

Here I would like to express my heartful gratitude to my supervisor Dr. Liu Bo, for his constant advice, guidance and warmest encouragement without whom none of this work could have been done. I would also gratefully acknowledge the kind support from my co-supervisor Prof. Chong Tow Chong.

Many thanks are given to Dr. Song Yunfeng and Mr. Zhou Jiang for their kind help with optical technology, Dr. Wan Lei for his advise on signal processing, Dr. Ma Yansheng for his direction on simulation study, Dr. Yuan Zhimin for his patient instruction and suggestion. Thanks are also given to my friends and colleagues, mentioned here in no particular order of Ms. Ye Huanyi, Ms. Kek Eeling, Ms. Liu Jin, Ms. Zhu Jin, Ms. Xiao Peiying, Ms. Zhou Yipin, Mr. Han Yufei, Mr. Li Hui and so on, for providing friendship and companionship through good and bad times.

I am not forgetting all the people in the Data Storage Institute (DSI). Further, I would thank DSI for the first class working environment and facilities.

I would specially thank the National University of Singapore and department of Electrical and Computer Engineering for the Research Scholarship. Finally, many, many thanks are given to my husband, my sister and my parents for their unwavering support throughout the years.

# Content

# Summary

The growing technology and economical importance of massive data recording in today's information era demand inexpensive, highly reliable, quickly accessible and high capacity (or high density) data storage systems. Magnetic hard disk drives are the only high capacity storage devices that can meet all those requirements at the lowest cost. In hard disk drives, one of the most important and effective approaches for increasing areal density is to position the read/write head closer to the surface of disk media, or to reduce the flying height of the read/write head over the recording disk medium.

Currently flying height has been reduced down to 8~10 nm for achieving an areal density up to 60~80 Gigabit per square inch ($Gb/in^2$). Researchers are pushing the technology towards 1000 $Gb/in^2$ which needs a flying height less than 3nm. Excessive flying height impairs the ability of the head to read or write data while insufficient flying height causes the head to hit the surface of the spinning disk and destroys the magnetic coating (and the data) on the disk. Therefore, making precise flying height measurement becomes more and more important and critical for the design and quality control of future magnetic data storage systems.

At present, the state-of-the-art technology for flying height measurement is optical interferometry including three-wavelength and polarization intensity interferometry methods. Comparing the two methods, the three-wavelength is superior to the polarization intensity interferometry. It is based on the conversion of detected light intensity into a value of spacing through the comparison of detected light intensity with a theoretical curve. The detected light intensity should be normalized according to the calibration curve which is obtained by calibration process before flying height

testing. The calibration is to find the maximum and minimum light intensity of the interference. Any error in the calibration process will affect the accuracy of flying height reading.

The cut-off frequency of the photodetector in flying height tester and the optical filter bandwidth of the flying height tester can distort the maximum and minimum interference intensity, thus, the calibration accuracy. Work presented in this thesis is mainly focused on tracing down and eliminating such errors.

A modeling platform was developed for both the evaluation of optical flying height testing technology and the virtual confirmation of new approaches to improve the testing accuracy. It is used to analyze the calibration error caused by the effect of cut-off frequency of the photodetector and optical filter bandwidth.

Systematic experiment studies were performed to investigate the limitations of current calibration method especially for sliders with strong negative pressure, which represents the future trend of slider technology.

Considerable work was carried out to explore the possible calibration error caused by the cut-off frequency response of the photodetector and how to compensate such error. Using the data obtained from numerical simulation, the performances of loading and unloading processes are both studied. Results show that the calibration error is more significant when using negative pressure slider with suspension limiters. Moreover, the impact of cut-off frequency of the photodetector is also studied under different light wavelengths and loading/unloading vertical velocities. Results show that reduced vertical velocity of slider loading and unloading can reduce the calibration error. A cut-off compensation method is proposed. Results suggest that the proposed compensation scheme is effective in terms of improving the calibration accuracy.

Further study extends to the investigation of optical filter. Experiment results show that wider bandwidth optical filter is good at improving signal quality. However, non-zero bandwidth of optical filter can also cause errors in calibration process. An integral response method is thus proposed and a new theoretical curve can be thus obtained. Results show that the new method can greatly reduce the calibration error. The integral response method also allows the use of optical filters with even broader bandwidth. Experimental data exhibit that the broader bandwidth optical filter and new theoretical curve can greatly improve the repeatability of flying height testing results.

# List of Figures

# List of Tables

# List of Abbreviations

| | |
|---|---|
| HDD | Hard Disk Drive |
| MB | Megabyte |
| GB | Gigabit |
| FH | Flying Height |
| MR | Magneto Resistive |
| L/UL | Loading/Unloading |
| TMR | Track Misregistration |
| $PW_{50}$ | Pulse Width at 50% of Peak Value |
| HGA | Head-Gimbal Assembly |
| PSI | Polarisation Interferometry |
| GUI | Graphic User Interface |
| CML | Computer Mechanics Laboratory |
| CSS | Contact-Start-Stop |
| VCM | Voice Coil Motor |
| A/D | Analog-to-Digital |
| FIR | Finite Impulse Response |
| PSA | Pitch Static Angle |
| RSA | Roll Static Angle |
| ABS | Air Bearing Surface |
| SNR | Signal-to-Noise Ratio |

# Chapter 1

# Introduction

## 1.1 Hard Disk Drive Development History

Magnetic data storage technology has been playing a key role in computer development since the beginning of computer technology [1]. The future of computer technology lies not only in increasing the computing power but also in providing the maximum amount of information at the lowest cost. For those reasons, there is a large demand for high capacity storage devices with low access time and cost. As of today, magnetic hard disk drives (HDD) are the only high capacity storage devices that can meet these requirements at the lowest cost.

To be competitive in this fast-paced environment, hard disk manufacturers must continually speed up product development. Figure 1.1 shows the evolution of hard disk drive in terms of capacity over these few years. For many years, engineers have improved them in every aspect: reliability, capacity, speed, power usage, and more. The key technological breakthrough that enabled the creation of the modern hard disk came in 1950s. In 1956 IBM built the first magnetic hard disk drive featuring a total storage capacity of 5 Megabyte (MB) at a recording density of 2 kbit/in$^2$. A hard disk drive for a personal computer system in 1992 had a capacity of 100 MB. By 1996, the technology development makes the hard disk drive capacity increased to 1.2 Gigabit (GB). Today's 3.5 inch form factor drives are of storage capacity of 80~120 GB per disk platter and total capacity of 80~240 GB per disk drive.

High areal density also makes it possible to reduce small form factor disk drives for magnetic data storage. The recently induced 1 inch micro-drives, which are used for consumer applications such as digital cameras, personal communications devices and hand held computers, can offer a storage capacity of 5 GB.

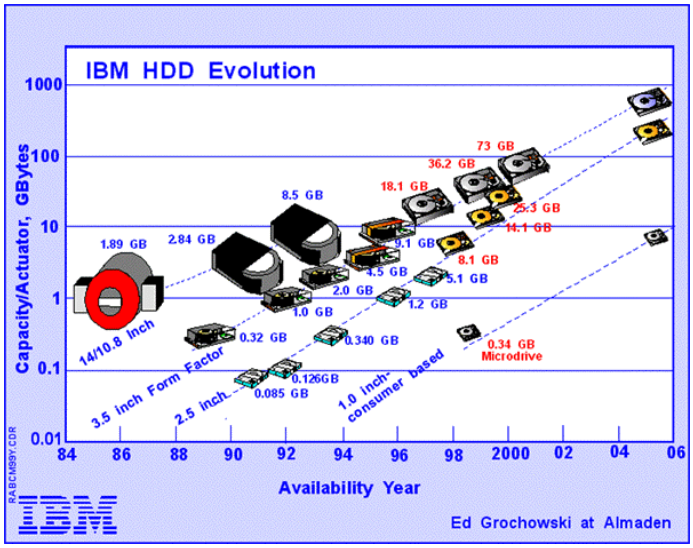


**Figure 1.1 Evolution of hard disk drive**

## 1.2 Hard Disk Drive Structure

Basic components of a hard disk drive are the read/write heads and the disks, as shown in Fig. 1.2. The read/write heads are too small to be used without attaching them to a larger unit. Therefore, each read/write head is mounted to a slider. The function of the slider is to physically support the head and hold it in the correct position relative to the platter as the head flies over its surface. The slider is attached to one end of the suspension. The other end of the suspension is attached to the actuator arm which is mounted to a ball bearing pivot structure on the drive case. The air pressure generated by the spinning disk makes slider flying. The head is held off the disk's surface by an air cushion, or air bearing. The characteristics of the air

bearing have a direct relationship with the aerodynamic design of the slider. The spacing between top of the magnetic layer and bottom of the read/write element mounted on a slider is called magnetic head-disk spacing. It includes the following components: disk overcoat thickness, lubricant, flying height (FH), slider overcoat thickness and pole tip recession of read/write transducers. Here, flying height refers to the spacing between the mean plates of disk surface profile and slider surface profile [2].

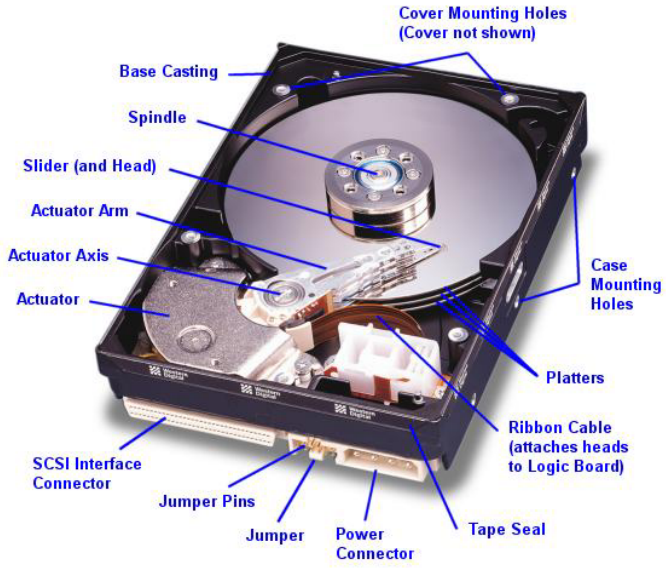


**Figure 1.2 Hard disk drive structure**

## 1.3 Relationship between Flying Height and Areal Density

Disk drive performance is usually measured by how many bits can be stored per unit area of a storage surface. The measurement of such performance is called areal density. Areal density (measured in bits per square inch) is the product of the number of tracks per inch (track density) and the number of bit per inch (bit density). Magnetic recording research and development efforts will continue to be aimed toward achieving higher areal density. In the request to lower the cost and improve

the performance, it has increased more than 20 million-fold in modern disk drives and currently increasing at a rate of 60% per year, as shown in Fig. 1.3.

The next research target is to demonstrate extremely high density magnetic recording of 1000 Gb/in$^2$ or 1 Tb/in$^2$ by 2008~2009.

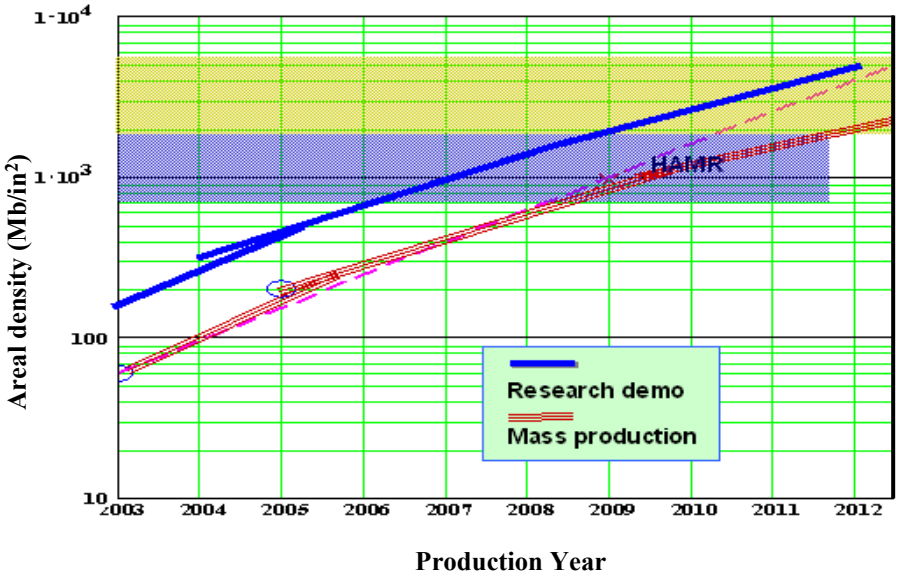


**Figure 1.3 Progress of areal density over past years**

Such a relentless quest to ever-higher areal density has been sustained, among other innovations and technological breakthroughs, by the continuing reduction of the mechanical spacing between head-slider and disk media. The smaller the head-disk spacing, the higher the read/write resolutions and, therefore, the higher the achievable areal density. At present, reading and writing heads are made in small size to conform to the higher track and bit densities that enable areal density to increase in a rapid speed. Because output signal declines proportionally with reductions in track width, new magneto resistive (MR) materials are developed to restore signals to acceptable levels above the noise. Moreover, signal pulses spread out and overlap adjacent pulse along the storage track; because increased bit density exacerbates pulse overlap and loss of signal, the spacing between the MR head and the disk must be reduced to

increase the strength of bit fields and store signals to useful levels. Currently technology allows for 8~10 nm flying height in high-end commercial disk drives. It is estimated that this would be reduced to around 2.5~3.5 nm to target at an areal density of 1 Tb/in$^2$, as shown in Fig. 1.4.

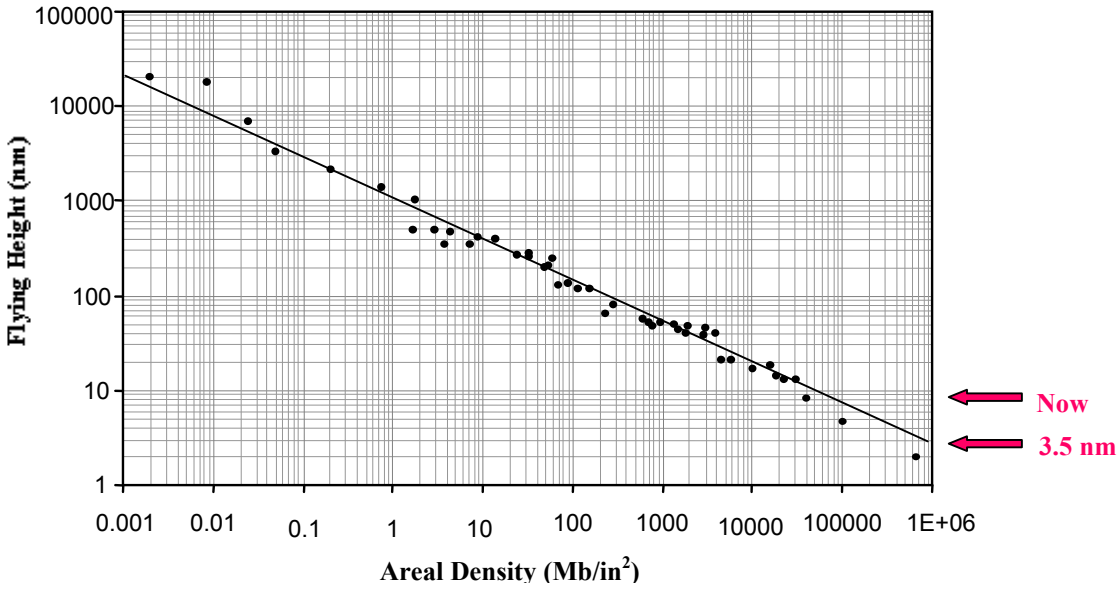


**Figure 1.4 Relationship between areal density and flying height**

## 1.4 Importance of Accurate Flying Height Measurement

At present, the flying height has been reduced below 10 nm. To realize such small spacing with high accuracy and high reliability, sophisticated technologies regarding fabrication, assembling, and process control are required. This means that flying height is valuable as an index which indicates up-to-date technology. Thus, the flying height, one of the major determinants of disk drive, must be checked not only during the stage of research and development but also throughout the manufacturing process. Flying height measurement has thus become an important technology in the disk drive industry [3]. Here, a frequently encountered problem in data storage system is the precise measurement of flying height near contact on a rapidly rotating rigid disk. The

closer the head flies over the disk surface, the higher the resolution of data is, and the greater the amount of data that can be stored. Excessive flying height impairs the ability of the head to read or write data, insufficient flying height causes the head to hit the surface of the spinning disk and destroys the magnetic coating (and the data) on the disk. Frequent head disk contact will deteriorate the tribological performance of the head disk interface and its reliability. Therefore, it becomes more and more important and necessary to make high accuracy head-disk spacing measurement.

## 1.5 Flying Height Measurement Methodologies

Over the past years, a variety of methods have been proposed to measure the flying height. Generally, the proposed methods can be classified into two categories: in-situ measurement methods and optical methods. In-situ flying height measurement methods include reading process based techniques and writing process based techniques. The reading process based methods include $PW_{50}$ method [4], all "1" harmonic method [5] and triple harmonic method [6]. The writing process methods comprise carrier erasure current method [7] and scanning carrier current method [8]. The optical interferometry technique mainly includes three-wavelength method [9-11] and polarization interferometry method [12]. A detailed review and analysis of these methods will be given in chapter 2.

Currently, the industry standard flying height testing technology is still based on the principle of optical interferometry, and the three-wavelength method is the only well established approach up to now.

## 1.6 Calibration of Flying Height Measurement

The three-wavelength method is utilized in the state-of-the-art flying height tester. It uses a calibration procedure in the flying height testing process [11]. During calibration, the slider is moved away from disk surface to an enough wide separation using some specified method. The purpose of this movement is to detect the maximum and minimum interference intensity which are obtained at the distance equivalent to a quarter of light wavelength and half of light wavelength.

The purpose of obtaining maximum and minimum intensity of calibration curve is to do the normalization. In the flying height tester, there are photodetectors which convert the intensity into electrical signals, and the electrical signals are then converted to digital data by A/D converter. In the whole system, the photoelectric conversion efficiency and the gain of photodetector are not very clear, so, the purpose of normalization is to eliminate such unclear relationships and simplify the whole measurement producer.

The procedure for measuring the flying height is as follows:

First, the slider is moved to the desired location over disk surface. Light is projected onto the head. The slider is then lift up from disk, so that a calibration trace can be generated. During the slider movement, the maximum and minimum intensity of the calibration trace are recorded by searching through the data collected. Following the calibration trace, a measurement trace is obtained. The trace will be normalized according to the maximum and minimum intensity of calibration trace. The measurement trace is scaled to 1 and the minimum intensity is scaled to 0.

Then the measurement of flying height is accomplished by comparing the normalized intensity with the normalized theoretical intensity versus flying height relationship, which is given in the following Equation

$$I_{normalized} = (I - I_{thry\max}) / (I_{thry\max} - I_{thry\min}) \tag{1.1}$$

$$I = \frac{r_{20}^2 + |r_{01}|^2 + 2r_{20}|r_{01}|\cos(\delta + \phi_s)}{1 + r_{20}^2|r_{01}|^2 + 2r_{20}|r_{01}|\cos(\delta + \phi_s)} \tag{1.2}$$

where, $\delta = \frac{4\pi h}{\lambda}$, $\phi_s = \pi - \tan^{-1}(\frac{2n_0k_1}{n_0^2 - n_1^2 - k_1^2})$, $r_{20} = \frac{n_2 - n_0}{n_2 + n_0}$, $r_{01} = \frac{n_0 - (n_1 + ik_1)}{n_0 + (n_1 + ik_1)}$, h is the flying height and λ is the light wavelength. $n_2$, $n_0$, $n_1$, $k_1$ are the refractive index of glass disk, air and slider material. $I_{thry\max}$ is the maximum intensity of theoretical curve and $I_{thry\min}$ is the minimum intensity of theoretical curve.

In sub-10 nm flying height region, accurate calibration of the slider flying height is a pre-requisite of accurate flying height measurement. The calibration consists of determining several different constants. The single most important source of error in the flying height measurement is associated with errors in the determination of the maximum and minimum interference intensities. Let us consider the error as $\Delta I_{\max}$ and $\Delta I_{\min}$ for the errors involved in the maximum and minimum intensities, respectively. The uncertainty in each of the quantities will propagate into the final result and limit the accuracy and repeatability of the measurement. These are called "calibration errors" [13].

Aside from some uncertainties that we always have in the measurement, such as noise, the calibration may be subjected to systematic errors, caused either by the effect of cut-off frequency of the photodetector or the optical filter bandwidth. A common effect of them is to distort the maximum and minimum interference intensities and thus introduce error to the final flying height testing results. Therefore, the systematic calibration errors must be traced down and eliminated by some certain methods.

## 1.7 Structure of Thesis

The structure of this thesis is as the followings:

**Chapter 1** states the background of the research work and gives an overview of the development of magnetic hard disk drives. The main challenges of accurate flying height measurement and possible calibration error are reviewed.

**Chapter 2** gives a detailed review and analysis of possible quantitative flying height testing technologies for flying height measurement in future hard disk drive manufacturing. A conclusion that optical interferometry, especially the three-wavelength method, as the most promising technology up to now, is obtained.

**Chapter 3** describes the development of a modeling platform for the evaluation of optical flying height testing technology. It is used to analyze the calibration error caused by the effect of cut-off frequency of the photodetector and optical filter bandwidth.

**Chapter 4** reports results of experimental investigations into the challenges and restrictions of the state-of-the-art flying height testing technology. The limitations of current calibration method are investigated especially for sliders with strong negative pressure.

**Chapter 5** explores the possible calibration error caused by the effect of cut-off frequency of the photodetector. Using the data obtained from modeling platform, the performances of loading and unloading processes are both studied. Results showed that the calibration error is more significant by using negative pressure slider with suspension limiters, and meanwhile the error produced in loading process is more significant than unloading process. In addition, the impact of photodetector's cut-off frequency is also studied under different light wavelengths and L/UL vertical

velocities. An error compensation method, the cut-off compensation method, is proposed and its feasibility is verified.

**Chapter 6** analyses another possible calibration error which is caused by the effect of optical filter. Instead of treating bandwidth of optical filter as disadvantages, this work dedicates on how to improve signal quality in flying height measurement and tries to benefit from the non-zero bandwidth of optical filter. An integral response method is then proposed. Obtained results indicate that taking bandwidth into account in signal processing and using reasonably wide bandwidth can both increase the intensity of testing signal and improve testing accuracy.

**Chapter 7** concludes this thesis and summarizes the main achievement.

# Chapter 2

# Flying Height Testing Methods

When the flying height is reduced to nanometer level, it becomes critical to accurately measure the head-disk spacing for implementing the design target of a reliable head-disk interface. Because of its importance, many contributions have been made to the development of methods for the measurement and characterization of the flying height.

The existing flying height testing technologies can be divided into two categories: in-situ methods and optical interferometry methods. The in-situ methods include reading process based techniques and writing process based techniques [14]. The reading process methods include waveform based approach and harmonic method. $PW_{50}$ method [4] is one of the most representative work of waveform method. The harmonic methods include all "1" harmonic method [5] and triple harmonic method [6]. The writing process methods comprise carrier erasure current method [7] and scanning carrier current method [8].

The optical interferometry experiences several important development stages since it is adopted as one major means to measure head-disk spacing. The 1$^{st}$ generation technology is monochromatic fringe counting technique [15]. The 2$^{nd}$ generation technology is white light interfeometry [15]. The 3$^{rd}$ generation is the three-wavelength method [16]. The method is easy to be implemented and can provide the best flying height repeatability. Therefore, it rapidly became the dominant flying height testing method. Another optical method investigated up to now is polarization

interferometry [12]. However, the method is not accepted by industry due to stress induced optical property change at a high spindle speed.

Aiming at identifying the most promising technology for future quantitative flying height measurement, these possible methodologies are reviewed and analyzed here.

## 2.1 In-Situ Flying Height Testing Techniques

In-situ flying height testing technology refers to the technology using the relationship between magnetic read/write signal and the head-disk spacing to measure the magnetic spacing of the head disk systems and to characterize the head disk interface [2]. As hard disk technology is driven towards 8~10 nm flying height, there exists high likelihood of causal slider-lube interaction and slider-lube-disk interaction [14]. Therefore, in-situ characterization of head-disk spacing and head disk interaction becomes a very attractive choice.

### 2.1.1 Reading Process Based Methods

The reading process based approach is established on the Wallace equation and Karlqvist head model [17]. It is assumed that the writing process is far less sensitive to the variation of head-disk spacing. Such an assumption is acceptable when the maximum head field acting on disk media is 2~3 times as high as medium coercivity.

The reading process based methods can be classified as two categories: waveform method and harmonic analysis method [14].

#### 2.1.1.1 Waveform Method

Waveform method detects the variation of head-disk spacing by the relationship between head-disk spacing and the shape of the isolated readback pulses [14]. Such a method is of significantly reduced sensitivity to the track mis-registration, comparing with the method based on analysis of the amplitude of readback signal. Furthermore, the effect of micro-fluctuation of media's remanent-moment-thickness product ($Mr\delta$) to the testing result can be small, comparing with the amplitude based method.

$PW_{50}$ is one type of the waveform based approach. $PW_{50}$ is the width of isolated pulse at 50% of its amplitude, a typical parameter to reflect the shape of the readback pulses [14]. This method is used for measuring static and dynamic flying height variations using the shape of the readback signal. Fig. 2.1 shows the waveform of the isolated pulses.

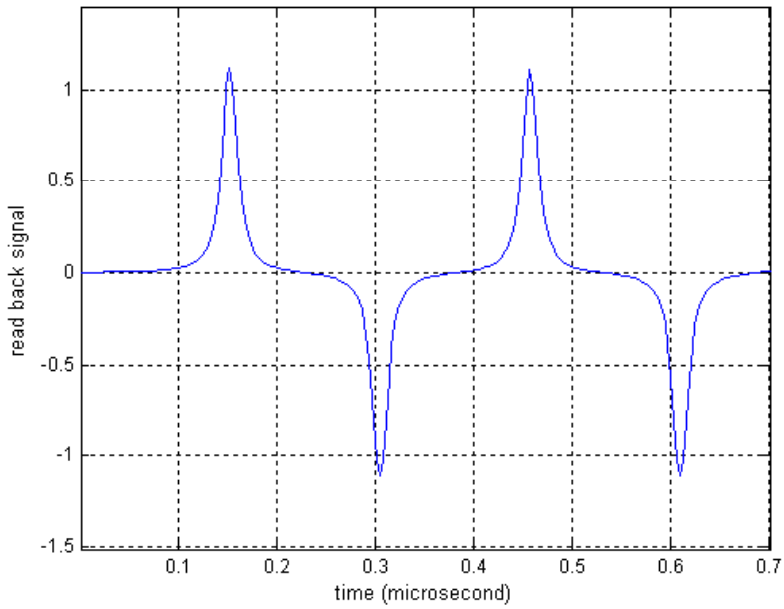


**Figure 2.1 Waveform of isolated readback pulses**

If the arctangent transition model and Karlqvist head field are valid, the general readback pulse width at half-amplitude for a thin medium can be expressed as [14]

$$PW_{50} = \sqrt{g^2 + 4(a+d)(a+d+\delta)} \tag{2.1}$$

where, $g$ is the head gap, $a$ is the transition parameter in the arctangent transition model, $d$ is the magnetic head-disk spacing and $\delta$ is the thickness of magnetic medium.

If a small gap Karlquvist head (g~0) is assumed, the $PW_{50}$ is simplified as

$$PW_{50} = \sqrt{4(a+d)(a+d+\delta)} \tag{2.2}$$

or if the thickness of medium is far less than gap length ( $\delta << d$ ), the $PW_{50}$ is given

$$PW_{50} = \sqrt{g^2 + 4(a+d)^2} \tag{2.3}$$

The isolated readback pulse can be approximated by the Lorentz Equation:

$$V = \frac{k}{1 + (\frac{2x}{PW_{50}})^2} \tag{2.4}$$

where k is a factor which is proportional to the track width, media's $Mr\delta$ value and the sensitivity of the reading head used.

The peak value of each readback pulse ($V_{peak}$) and the integration ($V_i$) of the isolated pulse can be expressed by the following equations:

$$\begin{cases} V_{peak} = k \\ V_i = \int_{-\infty}^{+\infty} V d_x = \frac{\pi}{2} k \cdot PW_{50} \end{cases} \tag{2.5}$$

The ratio of the integration to the peak value becomes proportional to the $PW_{50}$ only:

$$\frac{V_i}{V_{peak}} = \frac{\pi}{2} PW_{50} \tag{2.6}$$

The head-disk spacing can be estimated by the following equation assuming $\delta << d$ :

$$d = \frac{\sqrt{(\frac{2V_i}{\pi V_{peak}})^2 - 2g^2}}{2} - a \tag{2.7}$$

The $PW_{50}$ method is easy to be implemented and the noise in the integration waveform is small. Nevertheless, the sensitivity of this method is not high enough and the method has not been accepted as an established method for absolute flying height testing technology yet.

#### 2.1.1.2 Harmonic Method

The harmonic method uses the relationship between the amplitude of selected harmonic and the head spacing to characterize the head-disk spacing. The method is based on Wallace equation [17], which shows that the harmonic readback signal reduces exponentially as the head-disk spacing increases [14]. The harmonic amplitude of readback signal is also proportional to track width and $Mr\delta$ value of the media. Therefore, the effect of track width and $Mr\delta$ value must be removed in the testing process.

##### 2.1.1.2.1 All "1" Harmonic Method

As meant from its name, the all "1" harmonic method uses all "1" data pattern for in-situ flying height measurement [4]. The testing process is based on the amplitude ratio of the first and the third harmonics. The harmonic amplitude ratio can be expressed by the following Equation:

$$\frac{V_3}{V_1} = A_{31} k(g, \delta) \exp(-\frac{2\pi d}{\lambda}) \tag{2.8}$$

where, $A_{31}$ is the harmonic amplitude ratio factor, $k(g,\delta)$ is a factor determined by the gap length ($g$) of the read head and the medium thickness ($\delta$), λ is the recording wavelength, $d$ is the flying height.

$$d = -\frac{\lambda}{2\pi}\ln(\frac{V_3}{V_1}) \tag{2.9}$$

This method is required to test the flying height at a higher frequency in order to achieve higher flying height testing sensitivity. However, the flying height sensitivity is proportional to the channel density. A lower channel density will have lower sensitivity to the flying height variation. The problem of all "1" pattern is that the intensity of higher order harmonic signal is too low when comparing with that of its first harmonic, especially, at high user density, and the signal-to-noise ratio (SNR) of higher order harmonic is reduced. Therefore, the method is replaced by the triple harmonic method, as to be discussed.

#### 2.1.2.2.2 Triple Harmonic Method

A special code pattern of 111100 is recommended [18]. This method is called triple harmonic method as it provides three harmonics of comparable amplitude and energy intensity in a wide range of channel density. The proposed method is targeted to achieve improvement on both the amplitude level of the harmonics used for the spacing characterization and the sensitivity to the variation of the head-disk spacing.

The sensitivity of the proposed method can be expressed as:

$$\frac{V_3}{V_1} = A_{31}k(g,\delta)\exp(-\frac{4\pi d}{\lambda}) \tag{2.10}$$

$$d = -\frac{3\lambda}{4\pi}\ln(\frac{V_3}{V_1}) \tag{2.11}$$

The proposed method works at a channel density of 1.8 to 2.2 which is 6 times as high as the conventional method. The sensitivity to the variation of flying height is increased.

The major advantage of the proposed triple harmonic method is its large signal amplitude of its high harmonic component and the large amplitude of the higher harmonic signal gives stronger signal of the spacing variation. Another advantage of the method is its higher sensitivity to the flying height as it works at a higher channel density.

Triple harmonic method is the most promising approach in in-situ flying height testing technology. However, the technology still needs further development in order to become an industry accepted quantitative flying height measurement technique.

### 2.1.2 Writing Process Based Methods

The writing process based approach is designed to analyze the variation of the head-disk spacing during dynamic transient process, such as track seeking process and loading/unloading process where it is not so convenient in monitoring the pulse amplitude and not easy to remove the interference from off-track condition. It uses "erasure" operation on the pre-recorded data pattern to record the variation of the head-disk spacing during the transient process [14]. The writing process based method includes carrier erasure current method and scanning carrier current method.

#### 2.1.2.1 Carrier Erasure Current Method

Carrier erasure current method [7] is proposed to record the variation of the head-disk spacing caused by the dynamic operations, such as seeking, dynamic loading/unloading and head's take-off process.

Instead of basing the test on the readback process, the method uses a selected carrier erasure current to record spacing variation. Then, the recorded spacing variation is retrieved by readback operation with reading head at its static state — no relative motion between the head-gimbal assembly (HGA) and the base plate of the disk spindle.

The head-disk spacing and the spacing variation are recorded by the carrier current erasure operation in the form of bit cells. The spacing and spacing variation are retrieved through comparing the readback amplitude before carrier current erasure (the original amplitude) and the readback amplitude after carrier current erasure (the residual amplitude). The amplitude of both the original signal and residual signal is proportional to the corresponding magnetization difference between the magnetization in adjacent bit cells.

The magnetization difference after carrier current erasure is:

$$M_r - M = M_r - \frac{2M_r}{H_2 - H_1}(H_e - H_{er}) \tag{2.12}$$

The reaback amplitude before carrier current erasure ($V_0$) and after carrier current erasure ($V$) can be expressed as:

$$V_0 = 2M_r \cdot f(\beta_{head}, g, a, d_r, \delta) \tag{2.13}$$

$$V = f(\beta_{head}, g, a, d, \delta)[M_r - \frac{2M_r}{H_2 - H_1}(H_e - H_{er})] \tag{2.14}$$

where $f(\beta_{head}, g, a, d_r, \delta)$ is a factor describing the dependence of readback amplitude on head's magnetic coefficient $\beta_{head}$, gap length *g*, transition region length *a*, head-disk spacing during the readback process $d_r$ and the medium thickness $\delta$. Factor $f(\beta_{head}, g, a, d_r, \delta)$ will be of the same value no matter whether you are reading the original signal ($V_0$) or the residual signal ($V$) after carrier current erasure [7].

$$\frac{V}{V_0} = \frac{1}{2} + \frac{2g \cdot \Delta d}{\eta \cdot [g^2 + 4(d_0 + \delta)^2] \tan^{-1} \frac{g}{2(d_0 + \delta)}} \tag{2.15}$$

This method leads to a unique advantage of supporting all kinds of post-processing of the recorded spacing variation, aiming to filter out the influence of different types of interference caused by other factors. The method has the advantage of high sensitivity and easy to be implemented as it is based on amplitude measurement in the retrieval process of the recorded spacing range, selectable sensitivity and test range of the head-disk spacing. Unfortunately, the spacing testing range of this carrier erasure current method is still small and can't meet the requirement for head disk interaction analysis in loading/unloading process.

#### 2.1.2.2 Scanning Carrier Current Method

The scanning carrier method [8] uses "writing" or "erasure" operation to record the variation of the head-disk spacing during such transient processes. The recorded spacing variation is retrieved by reading operation and the effects caused by possible head-disk spacing variation in retrieval process must be small.

The pre-recorded magnetic transitions will not be affected at the time/position when the scanning current is zero. The readback signal from this position serves as a

reference signal in the flying height retrieval process. The phase variation of the scanning current is recovered by detecting the envelop of the readback signal. As the amplitude of the scanning current is known, the current value applied in scanning current erasure process can be derived based on the retrieved phase information. Therefore, the variation of coercive current in each cycle of carrier current scanning can be derived. Here, the coercive current is the value of carrier current which makes the readback signal reduce to half of its original value. In other words, the coercive current is the current value which generates a head field over disk media equal to its coercivity. The media coercivity is assumed to be constant and the head field can be described by Karlquist equation. The variation of head-disk spacing can be obtained from the following equation [8]:

$$\frac{I_{c0}}{I_c} = \frac{\tan^{-1}\left(\frac{g/2}{d_0 + \Delta d + \delta}\right)}{\tan^{-1}\left(\frac{g/2}{d_0 + \delta}\right)} \tag{2.16}$$

$$d = \frac{g}{a\tan\left[\frac{I_{c0}}{Ic}\tan^{-1}\frac{g}{2(d_0 + \delta)}\right]} \tag{2.17}$$

where $I_{c0}$, $I_c$ are the coercive current in track following status and the coercive current on the transient process, $d_0$ and $d$ are the head-disk spacing at track following status and the head-disk spacing in the transient process under investigation ($d=d_0+\Delta d$).

This scanning carrier current method has the advantage of large testing range in flying height measurement and is more suitable to the flying height and slider-disk interaction measurement in loading/unloading process.

## 2.2 Optical Intensity Interferometry Technique

Optical interferometry techniques use a transparent glass disk to replace the magnetic disk for the flying height measurement of head-slider [19]. Such a replacement is acceptable in terms of evaluating the flying performance of head-slider. The flying height is then determined by analyzing the interference phenomena between the head and disk [20].

### 2.2.1 Monochromatic Light Source Intensity Interferometry

Currently because white light is still used as light source of flying height testers, to understand how the interference pattern created by a white light source is interpreted, interference in a thin film created by a monochromatic light source should be investigated first.

The operating principle of monochromatic system is straightforward: A mechanism loads the slider onto a rotating glass disk, the light source illuminates a measurement point on the slider surface, and the thin-film effect modulates the reflected light [20]. Over portions of the modulation curve, it is possible to determine flying height by measuring the reflected intensity.

Fig. 2.2 schematically illustrates the working principle of the optical interferometry. The refractive index of glass disk, air and slider are $n_2$, $n_0$ and $n_1$ respectively. Monochromatic light is incident on this thin film. A portion of the incident light AE is reflected at the glass disk surface, while the remainder AB is refracted and transmitted through the glass disk into the air film. At the lower boundary of the air film, the transmitted light BC is reflected back through the air film. Because the head slider is made of opaque material, there is no light transmitted from the air film into slider. At

glass disk-air film interface, a portion of light CF is transmitted into glass and another part is reflected back again. The AE and CF combine to form an interference pattern.

The following discussion uses the interference between AE and CF light beams as an example to describe the basic working principle of optical inteferometry.

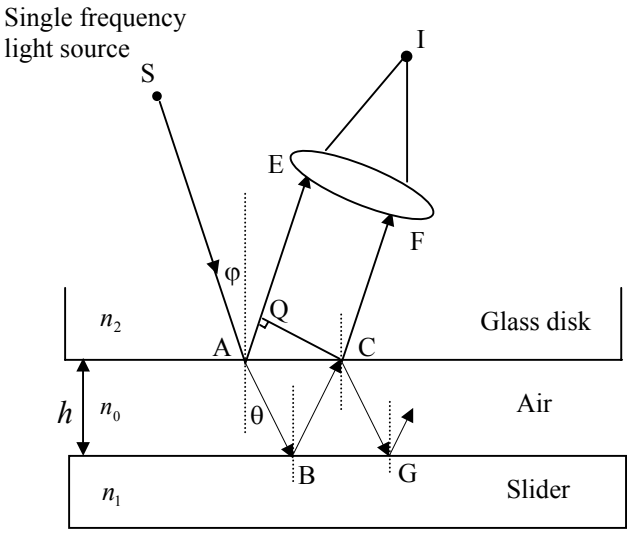


**Figure 2.2 Working principle of optical interferometry with monochromatic light**

The optical path length difference caused by two contiguous lights is $\Delta = AB + AC - AQ$ and the corresponding phase difference is $\delta = \frac{4\pi}{\lambda} n_0 h \cos\theta$. If these two lights AE and CF are in phase, maximum reinforcement occurs, whereas if they are out of phase, the reinforcement diminishes until total annihilation occurs when the phase difference is $180^o$. Total reinforcement or constructive interference results in a maximum light intensity and occurs when the optical path length difference is

$$\Delta = m\lambda \text{, (m integer)} \tag{2.18}$$

Annihilation or destructive interference, which results in a minimum light intensity, occurs when the optical path length difference is

$$\Delta = (m + \frac{1}{2}\lambda) \text{, (m integer)} \tag{2.19}$$

Therefore, given the refractive index of air is 1, as the h increases from zero, the intensity increases to a maximum at a separation equal to λ/4. It then decreases till another minimum is encountered at $h = \lambda / 2$, etc. So, the bright interference fringes are located when

$$h = \frac{2m+1}{4}\lambda \text{, (m integer)} \tag{2.20}$$

and the dark interference fringes will be located when

$$h = m\frac{\lambda}{2}\text{, (m integer)} \tag{2.21}$$

Monochromatic interferometric intensity is a periodic function of spacing, the "fringe order" must be known to finally determine the spacing. So it is limited by the periodicity of the interference, which introduces ambiguities and a severe loss of measurement sensitivity near contact. To overcome these problems, a variety of so-called white-light systems are available.

### 2.2.2 White Light Source Using Color Distribution Technique

With a white light source, the interference pattern from a thin film consists of a continuous color spectrum instead of the dark and bright fringes of the monochromatic pattern. Scanning through a range of wavelengths removes the periodic ambiguity and recovers measurement sensitivity over much of the flying height range, with the exception of very low heights near contact [21].

Therefore, for white light illumination, the color of the interference pattern at any point in the thin film is due to the superposition of those colors whose wavelength intensities are strengthened through constructive interference and the absence of those colors whose wavelength intensities are weakened due to destructive interference at that particular film thickness [21, 22]. From Newton's Color Scale [21], as shown in

Fig. 2.3, it is known that white light fringes are observable only up through the sixth or seventh fringe orders (1750 nm to 2000 nm). Also, as the fringes order increases, the resolution of the techniques decreases. The most useful operating range is from zero to the third or fourth fringe order (0 to 1000 nm). In this range the resolution is approximately 50 nm.

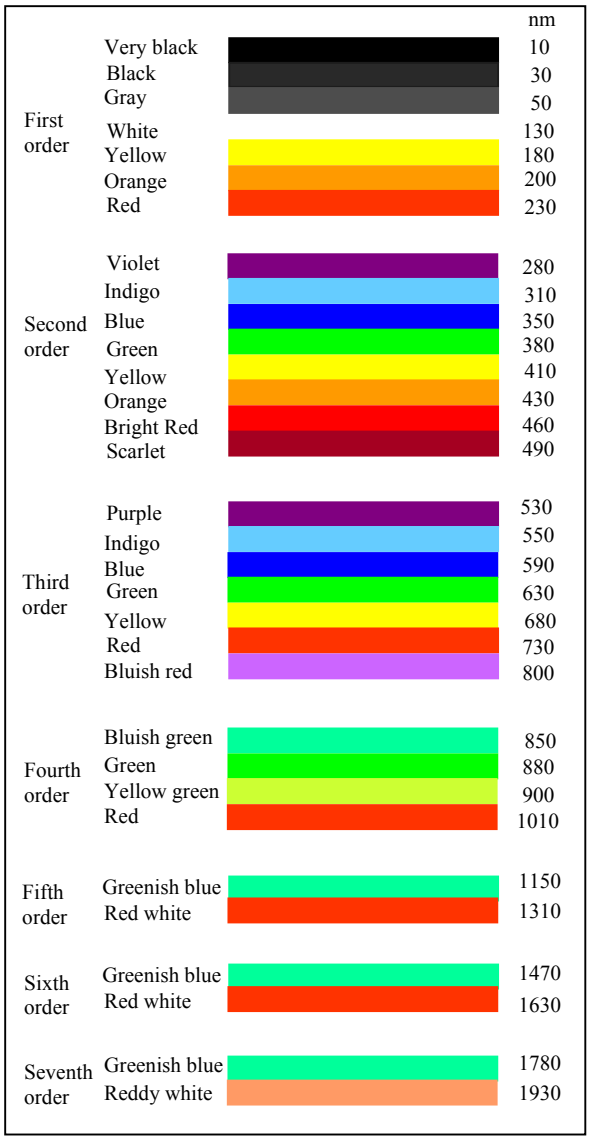


**Figure 2.3 Newton's color scale**

The film thickness for which white light interferometry is effective is limited, because the fringes are distinct only if the film thickness is not much larger than the

wavelength of the incident light [23, 24]. For any film thickness from zero to 500 nm, only a single wavelength in the visible spectrum gains maximum intensity. The colors are quite pure and distinct, except from 0 to 150 nm where the wavelengths in the visible spectrum reach their first intensity maximum so close together that the combined interference pattern appears as one fringe, changing from black to zero through gray to white at 125 nm before the first yellow occurs at 175 nm. From 500 nm to 1000 nm, there are two wavelengths in the visible spectrum that reach a maximum intensity at any given film thickness. From 1100 nm to 1500 nm, there are three such wavelengths. As the number of wavelengths that reach simultaneous maxima increases, the color of the interference fringe appears less distinct, until the superposition is so strong that the result is practically white illumination.

The main drawback of white-light system is that their process is slow and the detection resolution is too low. Constructive or destructive interference results in the generation of different color fringes which are compared to a Newton's color chart or analyzed by spectrometer. At spacings of less than 100 nm, the colors wash together and cannot be interpreted with reasonable accuracy. It also requires some time to acquire the intensity data which makes the slow measurement processing.

The solution to this problem is to settle on a small number of discrete wavelengths and measure the corresponding intensities, rather than scanning through the spectrum.

### 2.2.3 Three-Wavelength Intensity Interferometry Technique

The idea in the context of magnetic storage may be credited to Edwards, who in 1973 proposed a three-camera technique for simultaneous inspection of the tape drives at three discrete wavelengths. In 1992, a high-speed design for single-point

measurement was introduced [11]. The three-wavelength technique rapidly became the dominant technology for flying height testing.

Fig. 2.4 shows the schematic drawing of a three-wavelength monochromatic interferometer. Light source is directed through a beamsplitter. A portion of incident light split by the beamsplitter is directed through glass disk and internally reflected off the lower surface of the glass disk. Another portion of the light is reflected by slider. The reflected light is redirected into a detector assembly. The two reflected light beam combine to generate interference fringes, with one interference fringe being generated for each individual wavelength of light which has been selected by filters within the assembly. In the detector assembly, there is an optical filter in front of the photodetector. The interference filters are commercially available filters which transmit light at the chosen wavelength with a bandwidth. Therefore, the light source is optically coupled into a single beam using an optical filter and three distinct wavelengths are provided. The photodetecotor converts the fringes' intensity into electrical signals which are then converted to digital data. The digital data are then processed. Three measurements of three different wavelengths are combined using a weighted average to determined head-disk spacing.

The advantages of three-wavelength technique are as the followings.

It is insensitive to fringe order changes. It provides redundancy for measurements below the first order and can reduce the standard deviation of the measurement by a time factor of 1.5 to 2.5 as compared to a single monochromatic measurement.

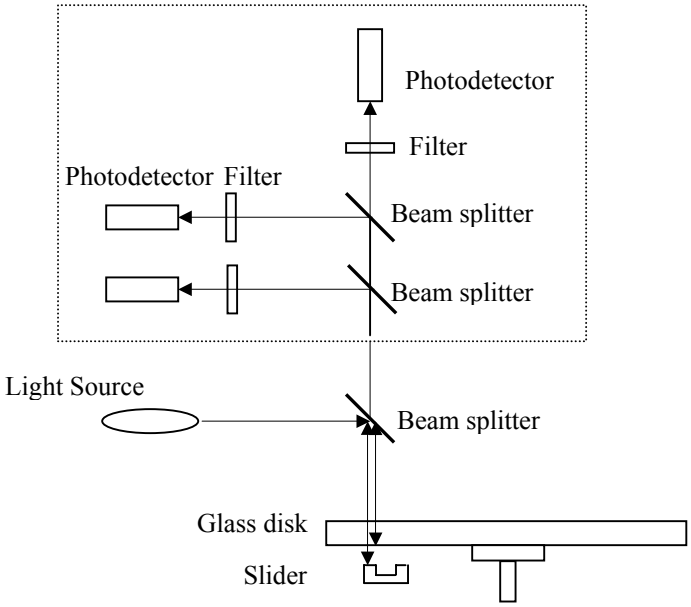


**Figure 2.4 Schematic drawing of three-wavelength flying height tester**

### 2.2.3.1 Single Reflection

Typically, sliders exhibit a single reflection at the surface [25]. Considering only the first two reflections and ignoring the rest is called a single reflection. As shown in Fig. 2.5, a beam of light *E* emitting from the light source transmits into the glass disk. The refractive index of glass disk, air and slider are $n_2$, $n_0$ and $n_1 + ik_1$, respectively. $k_1$ is the extinction coefficient of slider. Because the slider material $Al_2O_3$-$T_iC$ used here is not completely dielectric, the $k_1$ of slider is not equal to zero. At the glass-air interface, $E_{r20}$, a portion of *E*, is reflected back into the glass disk. The remaining light $E_{t20}$ transmits through the air spacing between the glass disk and the slider air-bearing surface. Similar to that at the glass/air interface, a portion of $E_{t20}$, labeled as $E_{r01}$, is reflected off at the air/slider interface. $E_{t02}$ of this reflected light transmits into the glass disk, and interferes with $E_{r02}$. For such a single reflection at normal incidence, the intensity of the interfered light beam is

$$I_s = I_{r20} + I_{t02} + 2\sqrt{I_{r20} I_{t02}} \cos(\frac{4\pi}{\lambda} h + \phi_s) \qquad (2.22)$$

Where, $I = \langle E^2 \rangle \equiv$ time average of the electric field square, $I_s$ is the intensity of the interfered light beam, λ is the wavelength of the ligth, $h$ is the spacing (flying height), and $\phi_s$ is the phase shift of light when it is reflected off the slider air-bearing surface. This phase shift is caused by the discontinuity of the light wave when it is reflected off the slider air-bearing surface. This phase shift can be calculated from

$$\phi_s = \pi - \tan^{-1}\left(\frac{2n_0 k_1}{1 - n_1^2 - k_1^2}\right) \tag{2.23}$$

This phase shift is $180^o$ (as if it occurs on a glass surface) if the $k_1$ is zero. As mentioned before, slider is made of $Al_2O_3$-$T_iC$ which is not completely dielectric and the corresponding $k_1$ is not zero. Therefore, the above equation does not yield a value of $180^o$ for $\phi_s$.

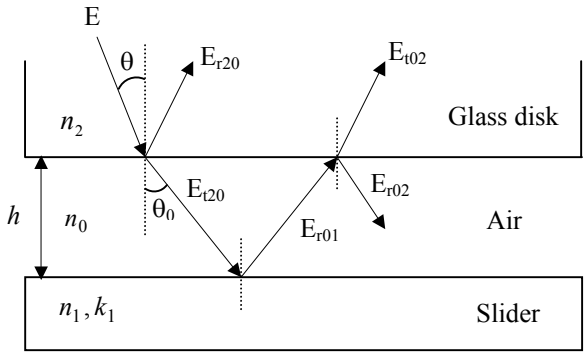


**Figure 2.5 Single reflection in head-disk interface**

### 2.2.3.2 Multi-Reflection

At a real hard-disk interface, a light beam experiences multi-reflection [16], as shown in Fig. 2.6. Therefore, the intensity of interfered light should be

$$I_s = I_0 \left| \frac{r_{20} + r_{01}\exp(i\delta)}{1 + r_{20} r_{01}\exp(i\delta)} \right|^2 \tag{2.24}$$

where, $\delta = \frac{4\pi h}{\lambda}\cos\theta_0$. For normal incidence, $\theta_0$ is equal to 90°. So, $\delta = \frac{4\pi h}{\lambda}$ $r_{20}$ is the reflection coefficient of the glass air boundary, $r_{01}$ is the reflection coefficient of air slider boundary, $I_0$ is the intensity of incident light.

For normal incident light,

$$I_s = I_0 \frac{r_{20}^2 + |r_{01}|^2 + 2r_{20}|r_{01}|\cos(\delta + \phi_s)}{1 + r_{20}^2|r_{01}|^2 + 2r_{20}|r_{01}|\cos(\delta + \phi_s)} \tag{2.25}$$

where, $\phi_s = \pi - \tan^{-1}(\frac{2n_0k_1}{1-n_1^2-k_1^2})$, $r_{20} = \frac{n_2 - n_0}{n_2 + n_0}$, $r_{01} = \frac{n_0 - (n_1 + ik_1)}{n_0 + (n_1 + ik_1)}$, $\delta = \frac{4\pi h}{\lambda}$, h is flying height.

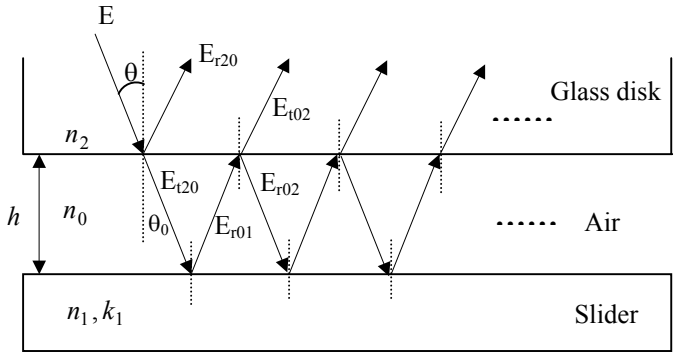


**Figure 2.6 Multi-reflection in head-disk interface**

Although the intensity of the reflected light decays very quickly after the first reflection, the importance of the multi-reflection can not be ignored. This is evident from Fig. 2.7, where the normalized intensities of the interfered light are plotted vs. flying height.

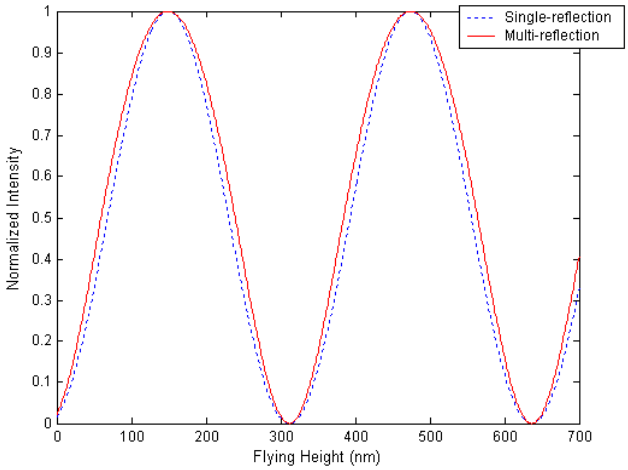


**Figure 2.7 Normalization intensity vs. flying height for a single and multiple reflection**

## 2.2.4 Polarization Interferometry

Laser based polarization interferometry is another interesting approach for optical flying height measurement. One major advantage of such technology is that of the potential of measuring slider's refractive index and flying height at the same time.

### 2.2.4.1 Dual-Beam Phase Shift Interferometry

Dual-beam phase shift interferometry (PSI) is known to be a method for nm level optical thickness measurement and with uniform sensitivity over the entire measurement range [26]. For conventional phase shift interfeometry, the reflection from the slider and the reflection from the disk surface must be separated. This is not easy because of the extremely small distance between the slider and the disk.

A dual-beam PSI geometry that avoids any disk coatings is then proposed [27]. A polarizing beam splitter divides the source light into two parallel beams with orthogonal polarizations [15], as shown in Fig. 2.8. Light source emits monochromatic beam which has two components of orthogonal linear polarization as indicated by the dot and arrow. Both beams are incident on the disk surface at

Brewester's angle ($\theta_B = \tan^{-1} n_2$, $n_2$ is the index of refraction of glass disk), so that one beam passes completely through the disk without reflection, while the other is partially reflected. The beam passing through the disk illuminates the slider, while the other beam serves as a reference. The two beams recombine to generate the familiar sinusoidal PSI signal. The image is of the interference pattern produced by the light wave reflected from the air bearing surface of magnetic head and the light wave reflected from the lower surface of glass disk.

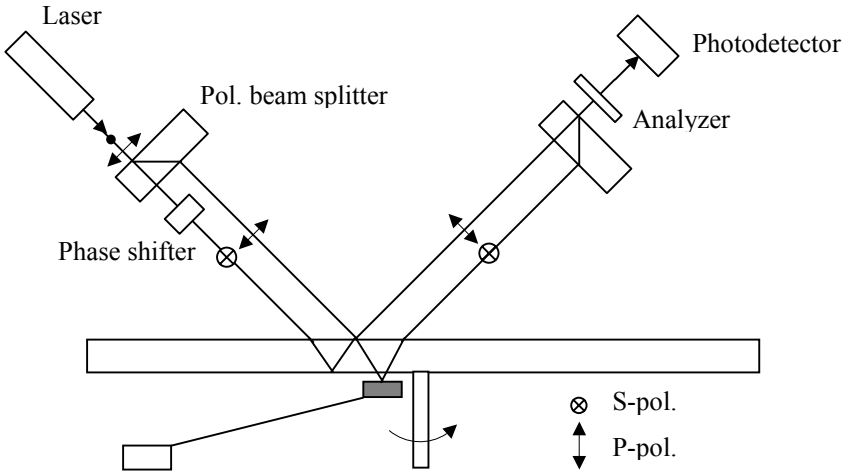


**Figure 2.8 Dual-beam phase shift interferometer**

Here again, however, there are important limitations that have slowed practical implementation. Most of these problems are associated with departing from the common-path geometry that makes traditional flying height testers insensitive to air turbulence and disk imperfections which will inevitably affect the measurement accuracy and resolution of whole system.

### 2.2.4.2 Polarization Interferometer

Despite the practical difficulties of PSI techniques, it still has made a convincing case for phase detection in flying height testers. Based on this, a new polarization interferometer method is proposed [28], as shown in Fig. 2.9.

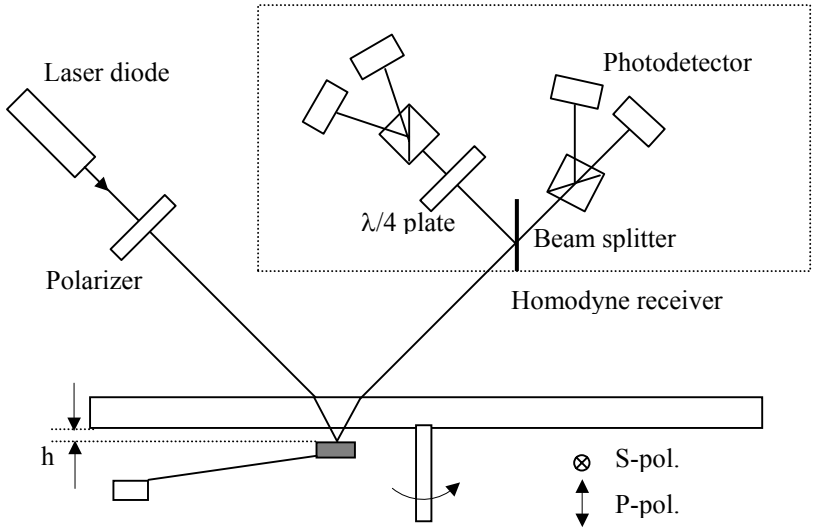


**Figure 2.9 Polarization Interferometer**

The theoretical basis of this tester follows from the standard equations for beam propagation in stratified media. The subscripts *p* and *s* denote the polarization states parallel and perpendicular to the plane of incidence; the effective reflectivities of the slider-glass interface are

$$Z_p(\beta) = \frac{r_p + r_{p'} \exp(i\beta)}{1 + r_p r_{p'} \exp(i\beta)} \tag{2.26}$$

$$Z_s(\beta) = \frac{r_s + r_{s'} \exp(i\beta)}{1 + r_s r_{s'} \exp(i\beta)} \tag{2.27}$$

where the phase term $\beta$ is given by

$$\beta = 2kh\cos(\theta) \tag{2.28}$$

The amplitude reflectivities $r_{s,p}$ are for the glass-air boundary, and $r_{s',p'}$ refer to the air-slider boundary. The phase $\beta$ depends on the wave number k=2π/λ, the angle of incidence $\theta$, and the flying height $h$. The normalized intensity of the reflected beam is

$$I(\beta) = I_s(\beta) + I_p(\beta) \tag{2.29}$$

$$I_s(\beta) = \left|z_s(\beta)\right|^2,\ I_p(\beta) = \left|z_p(\beta)\right|^2 \tag{2.30}$$

The phase difference between the polarization components of the reflected beam is

$$\theta(\beta) = \arg[z_s(\beta)] - \arg[z_p(\beta)] \tag{2.31}$$

Figures 2.10 and 2.11 shows the normalized intensity and phase difference as a function of flying height at an incident angle of 50 degrees. By inspection of these curves, one gains an immediate appreciation of the advantage of including the phase $\theta$ as a measurement parameter. The intensity and phase curve are complementary. When the intensity curve has a steep slope, the phase is fairly constant; when the intensity is nearly constant, the phase is changing rapidly. Using these curves together means that there is always a way to measure flying height with good snesitivity.

Polarization interferometer provides a means to measure the full complex reflectivity of the glass-slider interface. The independent measurement of refractive index of slider materials with ellipsometer is no longer required.

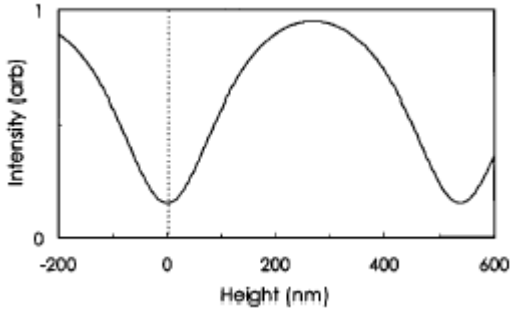


**Figure 2.10 Normalized intensity as a function of flying height**

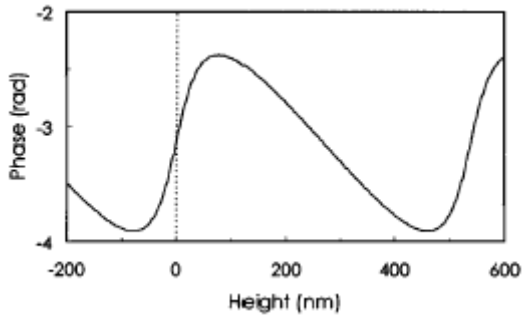


**Figure 2.11 Phase difference as a function of flying height**

The advantage of polarization interferometry is that it adds phase detection without giving up the traditional intensity information. Another advantage of polarzation interferoemtry is that it measures the refractive index of the slider in situ, using the data acquired during the slider load.

Nevertheless, this method still has some disadvantages. It has already shown that the beauty of the polarization interferometry is the added phase information. However, the phase measurement will be affected by many factors, such as noise sensitivity at contact and birefringence of glass disk. The glass birefringence is produced in the case of polarization interferometry and not easy to be corrected. The phase shifts induced by dynamic glass birefringence get mixed with the 'real' phase shift and add inaccuracy to the flying height measurement inevitably [29].

After considerable research, prototyping, data gathering and numerical evaluations, it is convinced that, given the present state of the art of recording head manufacturing technology, materials and other constraints, the three-wavelength method is superior to polarization interferometry [29].

## 2.3 Summary

In-situ flying height testing technologies are the only choice for drive level flying height analysis. However, the mature level of the technology has not put it for slider flying performance evaluation at production quality control yet. On the other hand, optical interferometry represents the technology for absolute flying height measurement methods.

The three-wavelength interferometry, the industry standard flying height testing technology is still the most mature choice at this moment and for recent future according to the evaluation of the possible technologies reported up to now.

# Chapter 3

# Simulation Program Results and Discussion

In this chapter, a modeling platform is developed for the evaluation of optical flying height testing technology. The accurate calibration is very important for accurate flying height measurement. The modeling platform is mainly used to analyze the calibration error caused by hardware setup of flying height testing system. One is photodetector and the other is optical filter. The further analysis of the effect of the two factors on flying height testing will be given in later chapters. Here, the software provides a convenient way to help us to have a fundamental understanding of them. By using the software, the magnitude of the calibration error and measurement error due to the different photodetectors with different cut-off frequencies and optical filter will be presented. In the simulation, only three layers of material are considered in the intensity interferometric. Finally, the simulation results will be discussed.

## 3.1 Effect of Photodetector's Cut-off Frequency on Flying Height Measurement

Currently, the negative pressure sliders are widely used in hard disk drive. The strong suction force produced by negative pressure sliders during unloading will affect the accuracy of calibration process. This is mainly due to the limited cut-off frequency of the photodetectors. As the existence of suction force, the slider' retracting process will be of high velocity. Therefore, it is possible that photodetector

can't detect the accurate maximum and minimum intensity. That will result in calibration error, which, in turn, will lead to flying height measurement error.

In general, a photodetector with lower cut-off frequency will lead to more significant error in calibration process.

### 3.1.1 Software Development

A Matlab-based GUI (Graphical User Interface) software, named DETECTOR, was developed to study the photodetector bandwidth impact on flying height measurement both in loading and unloading process, as shown in Fig. 3.1. A prerequisite which DETECTOR requires is that the flying height performance during loading and unloading process. This can be done easily by using the code developed by Computer Mechanical Laboratory (CML). Here, the software simulation is limited to three layers reflection—glass disk, air and slider.

The user needs to specify the refractive index ($n+ik$) of each layer and the wavelength used for flying height measurement. Moreover, the users need to set the parameters of digital filter including orders, cut-off frequency and sampling frequency which are used to represent the photodetector. Different results will be obtained by using different filters. By clicking **Reset** button, all the items in this GUI become blank. The users may, by clicking **radio buttons**, select to graph the calibration curve of unloading process or loading process. The two items are intended to be mutual exclusive of each other (only one button is in the selected state at any given time). To activate a radio button, click the mouse button on the object.

The calibration curve before importing photodetector parameters is called the ideal curve and the one after photodetector is called actual curve. Once the user enters all

the parameters and clicks the **Calculate** button, the GUI calculates the $\Delta I_{\max}$, $\Delta I_{\min}$ and $FH_{error}$ and displays the results in the **Results list**.

Here, $\Delta I_{\max}$ is the difference of the maximum intensity between the ideal curve and actual curve. $\Delta I_{\min}$ is the difference of the minimum intensity between the ideal curve and actual curve. In addition, the user can generate a graph of calibration curve during unloading or loading process by clicking **Plot** button. The GUI will be closed by clicking **Close** button.

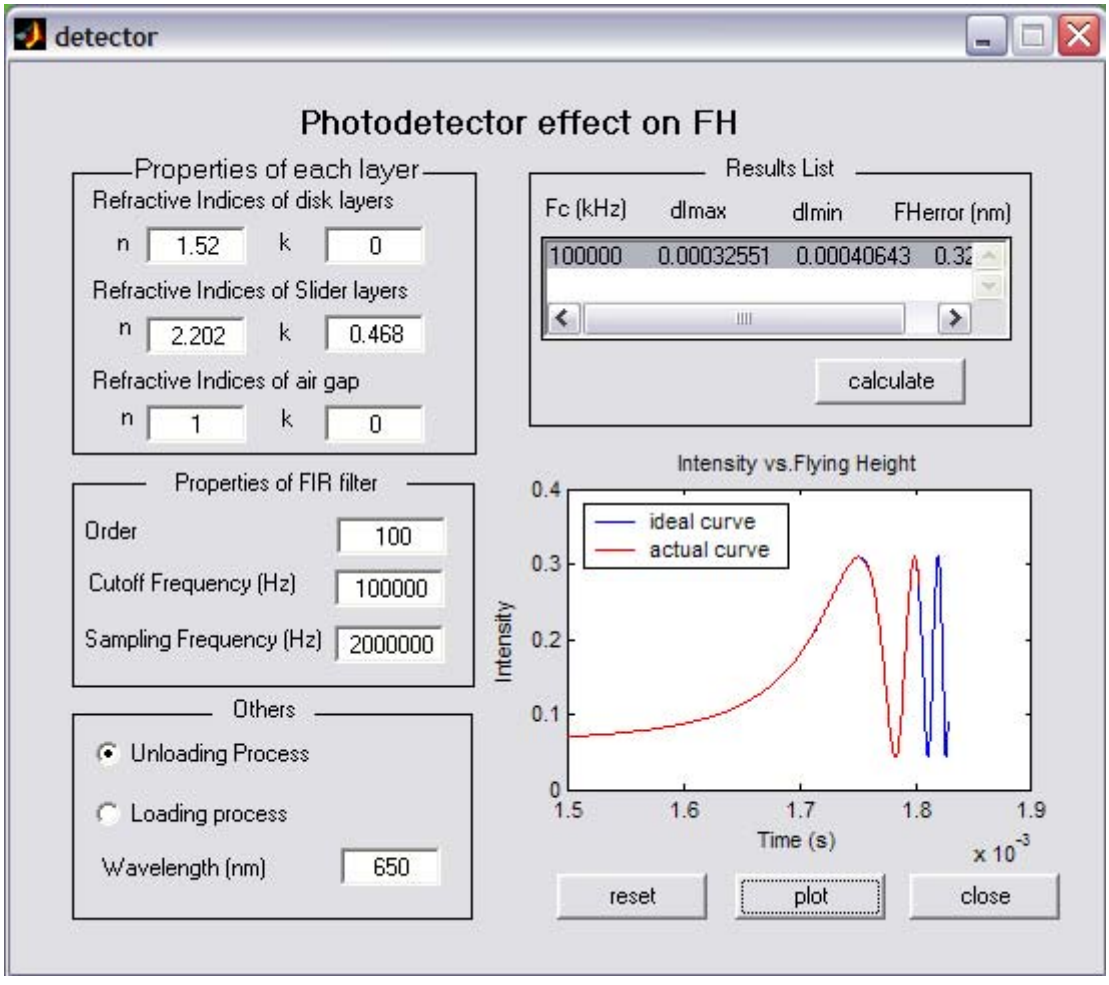


**Figure 3.1 User input window of DETECTOR**

### 3.1.2 Simulation Results and Discussion

Table 3.1 tabulates the calibration and measurement errors that are determined by DETECTOR for photodetectors with different cut-off frequencies. The light wavelength is 650 nm. It is observed that the $\Delta I_{\max}$, $\Delta I_{\min}$ and $FH_{error}$ decrease as bandwidth of photodetector increases in both loading and unloading process. The errors in minimum intensity are always larger than the error in maximum intensity. Furthermore, the errors produced in loading process are more significant than others in unloading process. These will be analyzed in detail in chapter 5.

**Table 3. 1 Simulation results of photodetector effect**

| | Cut-off frequency | $\Delta I_{\max}$ | $\Delta I_{\min}$ | $FH_{error}$ (nm) |
|---|---|---|---|---|
| Unloading Process | 90KHz | 0.000179 | 0.002044 | 0.821 |
| | 100KHz | 0.000152 | 0.000683 | 0.344 |
| | 110KHz | 0.000121 | 0.000312 | 0.272 |
| | 120KHz | 0.000026 | 0.000261 | 0.142 |
| Loading Process | 90KHz | 0.000308 | 0.000981 | 1.021 |
| | 100KHz | 0.000286 | 0.000709 | 0.491 |
| | 110KHz | 0.000213 | 0.000457 | 0.318 |
| | 120KHz | 0.000106 | 0.000326 | 0.254 |

## 3.2 Channel Response Effect on the Accuracy of Flying Height Measurement

The three-wavelength flying height testing technology works at three selected wavelengths. However, the light source is of wide spectrum. Therefore, it is necessary to have optical filters to select the targeted 3 wavelengths.

However, optical filter is still of a bandwidth. In other words, there always exists interference that comes from the neighbor frequency band of the targeted testing

frequency. The neighboring band interference causes the peaks and valleys of calibration curve to be attenuated. Attenuation means that the intensities of the peaks in the calibration curve are reduced and the intensities of the valleys are increased.

### 3.2.1 Software Development

A Matlab-based GUI program, named CRESPONSE, was developed to find out the calibration error and flying height measurement error caused by channel response impact, as shown in Fig. 3.2.

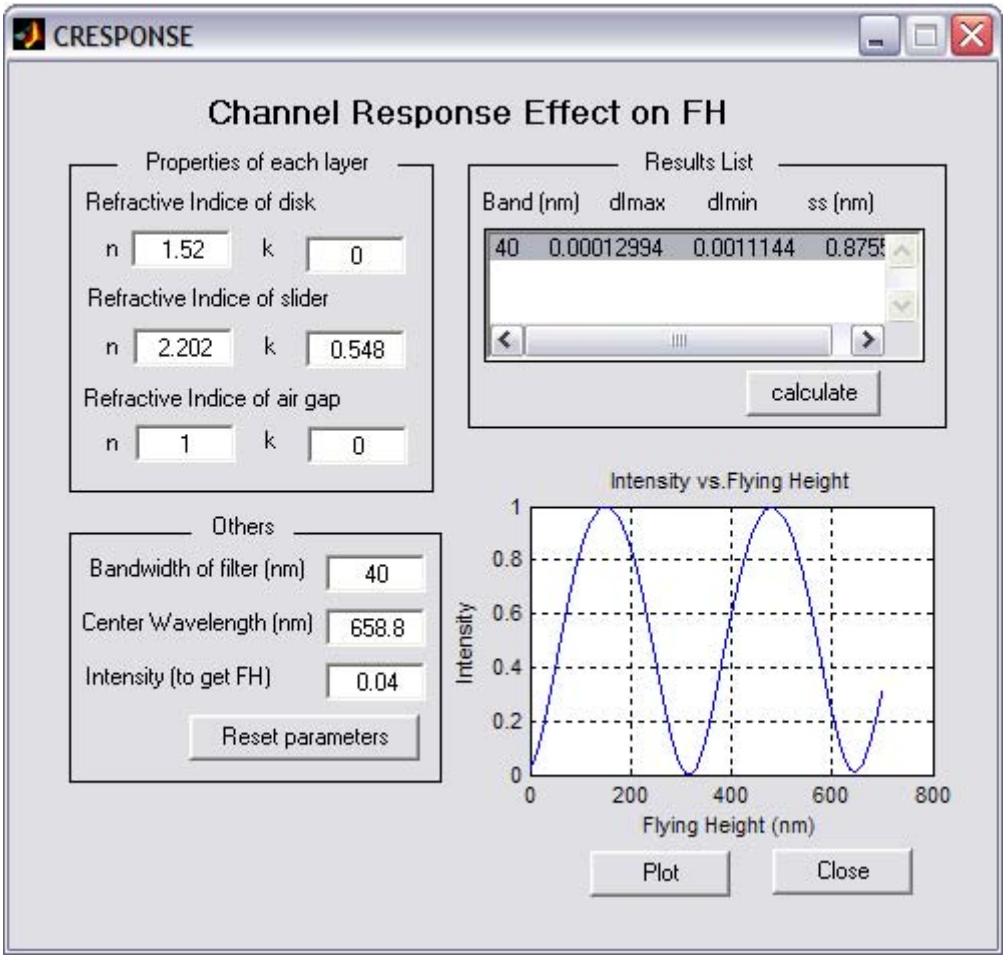


**Figure 3.2 User input window of CRESPONSE**

Besides the n, k value of each layer, the user needs to input other parameters which are the bandwidth of optical filter and the central wavelength of optical filter. By clicking **Reset parameters** button, all the items in this GUI become blank. The intensity vs. flying height curve produced by using one single central wavelength is regarded as the ideal curve. The curve generated by using non-zero bandwidth optical filter is regarded as actual curve. Once the user enters all the parameters and clicks the **Calculate** button, the GUI calculates the $\Delta I_{\max}$, $\Delta I_{\min}$ and $FH_{error}$ and displays results in the **Results list**. $\Delta I_{\max}$, $\Delta I_{\min}$ are the difference of maximum and minimum intensity between ideal and actual curve. The $FH_{error}$ is defined as the flying height difference between ideal and actual curve at a particular intensity level. The particular magnitude of intensity can be input as users want. In addition, the users may generate a graph of intensity vs. flying height by clicking **Plot** button. The GUI will be closed by clicking **Close** button.

### 3.2.2 Simulation Results and Discussion

As shown in Fig. 3.3, curve 1 illustrates the normalized intensity vs. flying height curve with zero bandwidth of optical filter. On the other hand, curve 2 (shifted to the left of curve 1) gives the normalized intensity vs. flying height when using non-zero bandwidth of optical filter. At a particular magnitude of light intensity, the flying height can be obtained. The spacing shift is defined as the spacing difference between curve 1 and curve 2 at the intensity level.

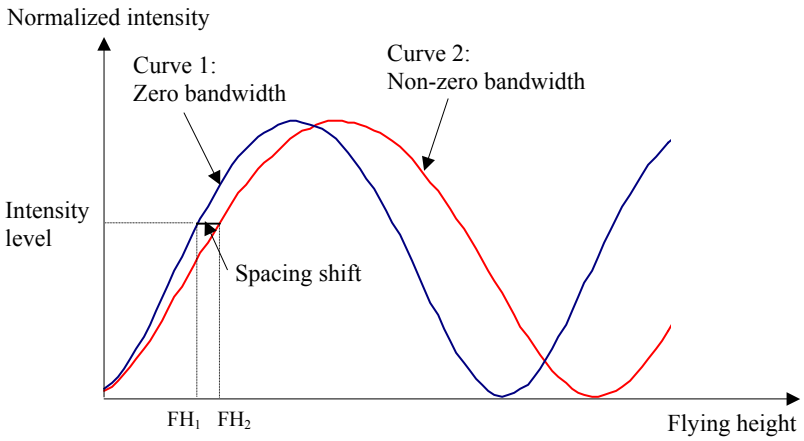


**Figure 3.3 Definition of spacing shift**

Table 3.2 tabulates the $\Delta I_{\max}$, $\Delta I_{\min}$ and $FH_{error}$ that are calculated by CRESPONSE for different optical filters. Wider optical filter bandwidth causes lager $\Delta I_{\max}$ and $\Delta I_{\min}$. The error in minimum intensity is more significant than the error in maximum intensity.

**Table 3. 2 Simulation results for different optical filters**

| | $\Delta I_{\max}$ | $\Delta I_{\min}$ | Spacing shift (nm) | | |
|---|---|---|---|---|---|
| | | | I=0.03 | I=0.04 | I=0.05 |
| 20 nm filter | 0.00003522 | 0.0002989 | 0.2726 | 0.2358 | 0.2104 |
| 40 nm filter | 0.00012994 | 0.0011144 | 1.0067 | 0.8756 | 0.7841 |
| 80 nm filter | 0.00050664 | 0.0042496 | 3.5939 | 3.1789 | 2.8778 |

## 3.3 Summary

A modeling platform has been developed to understand and evaluate the calibration error and measurement error caused by the effect of cut-off frequency of photodetector and optical filter bandwidth. It is found from the simulation that the calibration error and flying height measurement error are more significant when the

cut-off frequency of photodetector is low. On the other hand, narrower bandwidth of optical filter causes comparatively smaller error on calibration and accurate measurement of flying height.

# Chapter 4

# Investigation into Potential Problems in Calibration Process

## 4.1 Background

The need for a more reliable head-disk interface and lower flying height has been fueled by the need for ever increasing data storage capacity. Previously, contact-start-stop (CSS) technology was the mainstream design in disk drive industry. In a CSS drive, the air bearing slider is parked in a "landing zone" when the disk drive is not in operation. The slider stays at the landing zone during spinning up and spinning down, and moves to the data zone only when the disk rotational speed reaches operational condition [30]. However, the conventional CSS disk drive has difficulties in how to further reduce the carbon overcoat thickness and how to further reduce disk surface roughness.

Therefore, the technology is moving from CSS scheme to dynamic loading/unloading scheme. In the dynamic loading/unloading scheme, the head slider is at lift up (unload) status unless it is going to do read/write operation. For read/write case, the head will be released, or called loaded, onto disk surface. In such a scheme, the chance of slider-disk contact will be greatly reduced. Thus, this scheme allows thinner disk surface overcoat and smoother disk surface [31]. Some other advantages of dynamic loading/unloading include less power consumption and better non-operating shock resistance.

It has already been known that in order to obtain an absolute flying height value, it is necessary to compare the measured interference light intensity with a theoretical

curve when using three-wavelength flying height testing method. The measured intensity will be normalized to the maximum and minimum intensity of calibration curve [11]. The calibration process needs to move the testing point at least half wavelength above disk surface, aiming to test the maximum and minimum value of the light intensity. Such a flying height change is achieved by loading and unloading the slider to and from disk surface.

Currently, negative pressure air bearings are the only choice in hard disk drives due to its superior performance in stiffness, convenience in flying height profile control, small normal load and reduced sensitivity to altitude [30]. However, negative pressure may exacerbate the calibration error, which is a systematic error in flying height measurement. Therefore, it is necessary to confirm whether such effect is true and, if true, how to compensate.

The goal of this study is to investigate the potential problems of calibration during unload especially for negative pressure air bearing sliders. For comparison purpose, positive pressure sliders are used as a reference.

## 4.2 Mathematical Model

Form previous chapter, we got a general idea about calibration. Here, we use an example to further explain how to calibrate, how to calculate flying height when performing flying height testing, and more importantly how the error which is involved in the maximum and minimum intensity will influence the flying height value.

It is known that during flying height measurement, there is a calibration curve, also called calibration trace, followed by a measurement curve, also called measurement trace, as shown in Fig. 4.1.

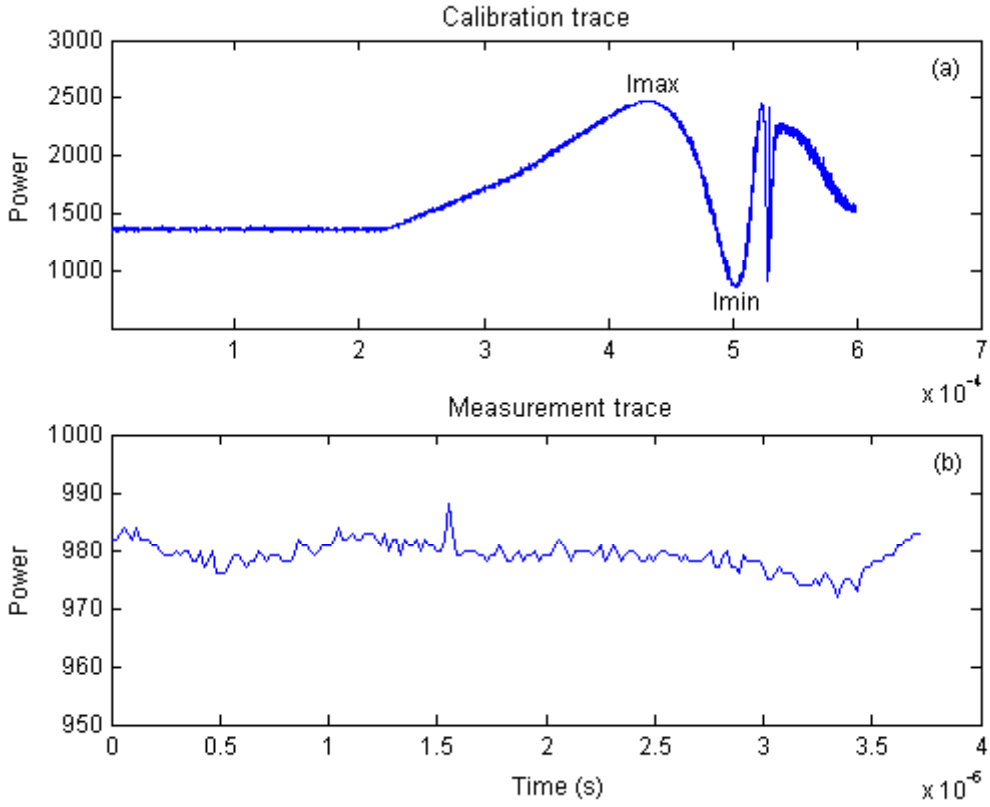


**Figure 4.1 Calibration trace and measurement trace in flying height measurement**

When calibration is performed, the slider is moved away from disk surface and the maximum and minimum interference intensity of calibration curve are recorded. The maximum and minimum intensity are obtained at the spacings equivalent to a quarter of light wavelength and half of light wavelength respectively. Following the calibration trace, the measurement trace is performed with the slider flying at a separation equal to flying height from disk surface. The measured intensity is normalized to 1 and 0 based on the maximum and minimum intensity of the calibration trace, as the following Equation

$$I_{normalized} = \frac{I - I_{\min}}{I_{\max} - I_{\min}} \tag{4.1}$$

where, $I_{normalized}$ is the normalized intensity; $I$ is the measured intensity. $I_{\min}$ and $I_{\max}$ are the maximum and minimum intensities of calibration trace.

Then the normalized intensity is compared with a normalized theoretical intensity vs. flying height curve to find the absolute flying height. The theoretical curve is obtained in advance by using interference light intensity resulting from multiple interference which is given as Equation 2.23. In low flying height region, the smaller the $I_{normalized}$, the lower the flying height.

In Fig. 4.2, there are two calibration curves. To facilitate the calculation, assuming that the $I_{\max}$ are the same, since at low flying height, the flying height calculation depends much on $I_{\min}$. In addition, if measurements are performed at the same conditions, $I$ are the same.

$$0 < I_{\min 1} < I_{\min 2} < I < I_{\max}; \tag{4.2}$$

$$0 < \frac{I}{I_{\max}} < 1; \tag{4.3}$$

According to (4.2) and (4.3), the following Equations can be obtained

$$\frac{I - I_{\min 2}}{I_{\max} - I_{\min 2}} < \frac{I - I_{\min 1}}{I_{\max} - I_{\min 1}} < \frac{I}{I_{\max}} < 1 \tag{4.4}$$

$$I_{normalized\,2} < I_{normalized\,1} \tag{4.5}$$

Hence, the flying height calculated based on calibration curve 1 is larger than the one based on calibration curve 2. So, the larger the peak-to-peak value, the higher the flying height.

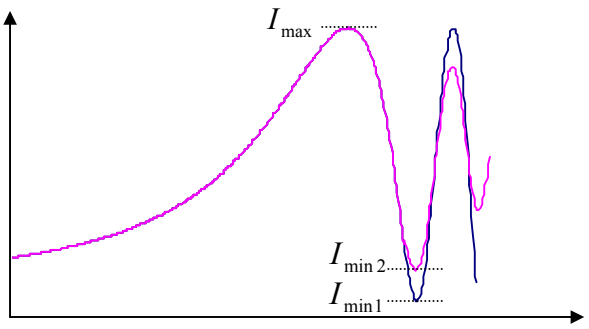


**Figure 4.2 Ideal and actual calibration curves**

## 4.3 Experiment Method

The purpose of the experimental investigation is to confirm quantitatively whether there is a change of the head-disk spacing when calibration is performed under different spindle speeds. The quantitative measurement of head-disk spacing is conducted with the industry standard flying height tester.

The following aspects are important in the experimental investigation.

The intermolecular level interactions happen only when the spacing between the slider and disk surface is small (say, less than 3 nm). Therefore, to let slider flying at head-disk spacing much higher than such a spacing value will make the spacing free from the disturbance caused by the intermolecular interactions [32].

Another is to fully benefit from the available resolution of the flying height testing system setup. According to the working principle of an optical interferometer, the head-disk spacing testing resolution of the dynamic flying height tester will be around its maximum when the head-disk spacing is around 25~70 nm. In addition, the obtained absolute value of flying height measurement error at such flying height is the same as the case when the flying height is only 3~4 nm, as it is a systematic error.

Therefore, the sliders with a flying height of 30~35 nm are selected.

Two types of sliders are used here. One is burnishing type sliders, which is one type of positive pressure slider and another is pico slider, which is a type of negative pressure slider, as shown in Fig. 4.3.

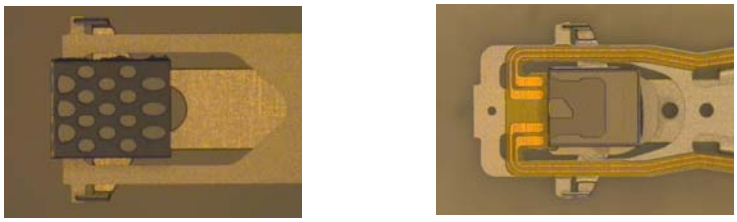

(a) (b)

**Figure 4.3 Two types of sliders used in the experiemental study**
**(a) positive pressure slider (b) negative pressure slider**

Based on unloading process, the retract calibration was used. All the flying height measurements were performed at 7000 rpm and a track of 30 mm radius with a zero skew angle. The values of spindle speed used for calibration are 6000 rpm, 7000 rpm, 8000 rpm, 9000 rpm and 10000 rpm, which correspond to a velocity of 18.84 m/s, 21.98 m/s, 25.12 m/s, 28.26 m/s and 31.4 m/s, respectively. The calibrations were also performed at a track 30 mm radius with a zero skew angle. All the testing results are obtained after more than 10 times averaging at each spindle speed. The disk and sliders were examined using a microscope to ensure that they are clean enough.

## 4.4 Results and Discussion

From tables 4.1 and 4.2, it is observed that the 1$^{st}$ peak, 1$^{st}$ valley, the peak-to-valley value of calibration curve and flying height at 6000 rpm are different from those when calibration spindle speed is up to 10000 rpm. The amplitude of the 1$^{st}$ peak, the maximum intensity, is raised and the level of 1$^{st}$ valley, the minimum intensity, is lowered at higher spindle speed. Also the peak-to-valley value increases.

Actually, the 1st peak, 1st valley and peak-to-valley are parameters which are not relevant to spindle speed, if it is viewed purely from optics point. Thereby, the variation of these parameters should come from the effects relevant to the increased spindle speed.

As shown in Fig. 4.4, the increased peak-to-valley value of calibration curve, caused by increased spindle speed, leads to an increase of flying height. This agrees well with the mathematical model. Furthermore, increased calibration spindle speed tends to a slightly increase of the amount of flying height. But, increased calibration spindle speed causes a more significantly increase of the amount of flying height increase when negative pressure slider is used instead of positive pressure slider.

The reason is given here. It has already been reported that as spindle speed increases, the lift-off force decreases [31]. Smaller lift-off force results in smaller lift-up velocity of slider. Due to the effect of cut-off frequency limit of the photodetector, the maximum and minimum intensities of calibration curve may be deviated from their real values if the slider is unloaded from disk with an increased velocity. The magnitude of maximum intensity is lowered and the level of minimum intensity is raised. In another word, the calibration will be more accurate at a higher spindle speed.

The positive pressure air bearing does not have negative suction force. With a suction force to hold the slider from unloading, the lift-off force becomes larger [33]. So, the negative pressure sliders are lift up faster than the positive pressure sliders. Therefore, the amount of flying height increase is more significant when negative pressure sliders are used rather than positive pressure sliders.

**Table 4. 1 Results of calibration curves of positive pressure sliders**

| Calibration | Blue | | | Green | | | Red | | | FH |
|---|---|---|---|---|---|---|---|---|---|---|
| rpm | Peak | Valley | Ip-p | Peak | Valley | Ip-p | Peak | Valley | Ip-p | (nm) |
| 6000rpm | 2220 | 894 | 1326 | 2548 | 953 | 1595 | 2419 | 824 | 1596 | 33.15 |
| 7000rpm | 2221 | 889 | 1332 | 2552 | 949 | 1603 | 2421 | 817 | 1604 | 33.20 |
| 8000rpm | 2222 | 886 | 1336 | 2554 | 944 | 1610 | 2427 | 815 | 1612 | 33.25 |
| 9000rpm | 2222 | 884 | 1338 | 2554 | 943 | 1611 | 2428 | 812 | 1616 | 33.31 |
| 10000rpm | 2223 | 882 | 1341 | 2555 | 941 | 1614 | 2428 | 810 | 1618 | 33.38 |

**Table 4. 2 Results of calibration curves of negative pressure sliders**

| Calibration | Blue | | | Green | | | Red | | | FH |
|---|---|---|---|---|---|---|---|---|---|---|
| rpm | Peak | Valley | Ip-p | Peak | Valley | Ip-p | Peak | Valley | Ip-p | (nm) |
| 6000rpm | 2119 | 903 | 1216 | 2496 | 980 | 1516 | 2441 | 866 | 1575 | 33.92 |
| 7000rpm | 2121 | 897 | 1224 | 2499 | 975 | 1524 | 2445 | 857 | 1588 | 34.20 |
| 8000rpm | 2122 | 893 | 1229 | 2502 | 968 | 1534 | 2449 | 852 | 1597 | 34.45 |
| 9000rpm | 2124 | 888 | 1236 | 2505 | 964 | 1541 | 2454 | 848 | 1606 | 34.68 |
| 10000rpm | 2126 | 882 | 1244 | 2507 | 960 | 1547 | 2459 | 841 | 1618 | 34.95 |

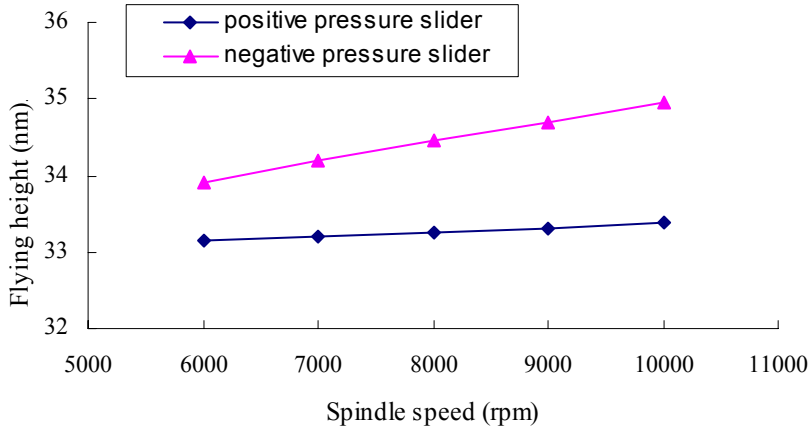


**Figure 4.4 Flying height vs. different calibration spindle speeds**

## 4.4 Summary

Negative pressure sliders represent the future of slider and air bearing technology. It is important to make sure that the flying height of such sliders can be measured

accurately. Results from experiment and modeling indicate that one concern in future flying height measurement is that the strong suction force of negative pressure slider will affect the accuracy of calibration process. Investigations in this experimental study reveal that the increased peak-to-valley of calibration curve, caused by increased spindle speed, leads to an increase of flying height, even when spindle speed is at its very normal range of 6000 rpm~10000 rpm. Using negative pressure sliders, the possible flying height testing error of current calibration process can be up to 1 nm which is too high for accurate determination of head disk spacing.

Such phenomenon and explanation have been further confirmed by comparative study of calibration induced flying height testing error between negative pressure slider and positive pressure slider. The experiment observation agrees well with mathematic model.

# Chapter 5

# Further Analysis of Cut-Off Frequency Effects of Photodetector on Flying Height Measurement

From chapter 4, it is known that the strong suction force produced by negative pressure slider during unloading process will affect the calibration process and results in calibration error and flying height measurement error. The error doesn't come from optics aspect but from the combined effect of slider's rapid motion in calibration process and the limited cut-off frequency of the photodetector.

In the future, negative pressure air bearing sliders with suspension limiters for dynamic loading/unloading applications will be the main choice of slider suspension technology. Therefore, it is necessary to thoroughly understand the impact of such a combined effect to the flying height measurement accuracy.

The goal of study in this chapter is to investigate the accuracy of calibration and flying height measurement when using negative pressure slider with suspension limiters. Both tri-pad positive pressure slider and negative pressure sliders with and without suspension limiters are included in the analysis. In comparison to the unloading process, the accuracy of calibration and flying height measurement in loading process are also studied to see which process (loading or unloading process) is more suitable for the calibration of flying height measurement.

## 5.1 Photodetector Model

When the slider is unloaded from the disk, the light reflected from the slider and from the surface of the disk is combined to form the interference fringes. The photodetectors within the detector assembly convert the fringe's intensity into electrical signals which are then converted to digital data by an Analog-to-Digital (A/D) converter and then processed by processor.

In order to investigate the effect of photodetector's cut-off frequency on the accuracy of calibration and flying height measurement, it is necessary to understand its characteristics first.

The frequency response of photodetector can be represented with a low-pass filter. The magnitude of the transfer function for a typical low-pass filter [34] is shown in Fig. 5.1.

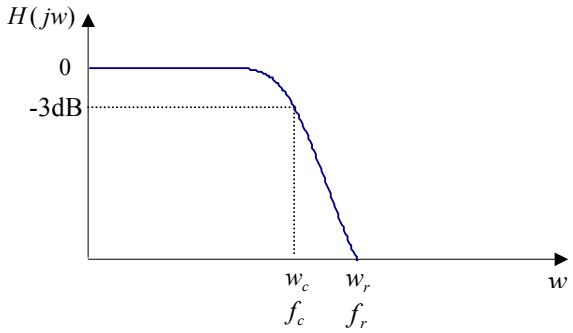


**Figure 5.1 Magnitude of transfer function of a low-pass filter**

where,
$$\left|H(jw)\right| = \frac{1}{\sqrt{1+(w/w_c)^{2n}}} \tag{5.1}$$

The low-pass filter passes low frequency signals and attenuates high frequency signals. The region $0 \le w < w_c$ is called the pass band, where the $\left|H(jw)\right|$ attenuates from 0 to –3dB. The angular frequency $w_c$ is called the angular cut-off frequency and

$f_c$ is called the cut-off frequency. The region $w_c \le w < w_r$ is called the transition band. The region $w_r \le w < \infty$ is called rejection band. $w_r$ is called the angular rejection frequency and $f_r$ is called the rejection frequency.

Signal that is a function of time can be represented by a combination of sinusoids and cosinusoids of various frequencies. This is called a frequency domain representation. The mechanism whereby signals are represented in frequency domain is the Fourier transform.

If the signal is not to be distorted by the low-pass filter, $|H(jw)|$ must be constant and phase must vary linearly with frequency over all the frequencies contained in the Fourier transform of signal. Here, the low-pass filter used is Finite Impulse Response (FIR) filter. It is a linear phase filter. There is no need to consider the phase distortion.

If all the frequencies present in the Fourier transform of signal lie within the region where $|H(jw)|$ is equal to a constant, the signal will be unaffected by the filter. However, the $|H(jw)|$ attenuates from pass band to stop band. Therefore as long as the frequency components of the Fourier transform of calibration curve falls in the region where $|H(jw)|$ begins to attenuate, the signal will be distorted, resulting in unavoidable error.

## 5.2 Simulation Results and Discussion

The simulation includes the following steps:

a) Simulate flying height variation in loading and/or unloading process.

b) The slider's flying performance in both loading and unloading processes are investigated using the slider's flying performance simulator developed by the

Computer Mechanical Laboratory (CML), University of California at Berkeley, USA. It is an industry standard simulator for flying performance analysis.

Both unloading and loading processes are studied with the intention to check which one is more suitable for calibration. Effects of loading/unloading vertical velocity and light wavelength are also studied.

The calibration and flying height measurement error in loading/unloading process when using negative pressure slider with suspension limiters are compared to the negative pressure slider without suspension limiters and a tri-pad positive pressure slider. Significant differences are found between these three types of slider-suspension systems.

As mentioned before, the negative pressure sliders have many merit features. However, the negative pressure will tend to keep slider close to disk surface in unloading process, which results in dimple separation in the dynamic unloading process and a longer time to unload, comparing with positive pressure slider case. Such a long unloading process decreases the recordable area of the disk, which is unacceptable. To overcome this, the hard disk drive industry employs negative pressure slider with suspension limiters. With limiters on suspension, the unloading time is greatly shortened, but the lift-off forces are increased [35]. That may result in another problem. With large lift-off force, the slider may be lift-up with a very large velocity. This results in calibration error and flying height measurement error, due to the limitations of cut-off frequency of photodetectors. To illustrate this problem, the above-mentioned three types of sliders are compared.

The air bearing surfaces of the three types sliders are shown in Fig. 5.2. Slider A is classic tri-pad positive pressure air bearing design with two front straight rails and a small pad located at the center of trailing edge. Slider B is the widely used pico

negative pressure slider. The slider B is mounted onto two types of suspensions. One case is without suspension limiters and the other case is with suspension limiters.

All simulations are performed at the disk radius of 36 mm with zero skew angle. The slider is loaded from an initial height of 30 μm over the disk surface. The disk rotates at 7200 rpm. The vertical velocity for both loading and unloading processes is 32 mm/s. All the cases shown here have 1° pitch static angle (PSA) and 0.5° roll static angle (RSA), which are typical values used in industry. The velocity of slider can be obtained by using Equation 5.2

$$v = (FH_2 - FH_1)/(t_2 - t_1) \tag{5.2}$$

The state-of-the-art flying height tester uses a photodetector with 0~100KHz bandwidth. Therefore, a low-pass filter with 100kHz cut-off frequency is used to represent the frequency response of the photodetector to study its impact on calibration and flying height measurement accuracy.

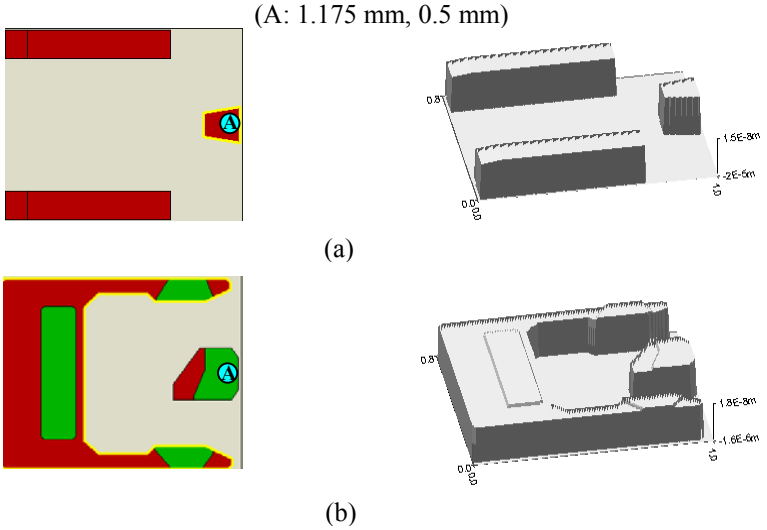


**Figure 5.2 Air bearing slider used in simulation**
**(a) positive pressure slider (b) negative pressure slider**

### 5.2.1 Slider Design and Unloading Process Based Calibration

During ramp unloading process, the actuator swings towards the ramp. After the lifting tab touches the ramp, suspension load beam moves upwards at a specified velocity. However, the air bearing slider can't move with suspension immediately. The slider is held by the suction force which is produced in head disk interface. When the deformed suspension flexure produced by stiffness overcomes the suction force, the slider can be lifted up. The amount of flexure deflection is referred as dimple separation [30].

The calibration process is to test the maximum and minimum light intensities. It needs to move slider over 1/2 of the maximum wavelengths of the selected 3 wavelengths.

The flying height and velocity profiles of these three types of sliders during dynamic unload process are shown in Fig. 5.3. As long as the slider is unloaded to 314 nm, the calibration procedure can be finished. Here, the flying height is at its range of 0~1000 nm.

The flying height and corresponding velocity profiles in unloading process of positive pressure slider are shown in Fig. 5.3 (a). It is found that it takes a very short time to finish the unloading process. That is because only a small amount of suction force is generated by tri-pad positive pressure slider which requires very small flexure force to unload it. The maximum velocity of positive pressure slider reaches 12.1 mm/s in the calibration period.

The flying height and corresponding velocity profiles in unloading performance of negative pressure slider without limiters are shown in Fig. 5.3 (b). The unloading time is significantly longer than positive pressure slider. There are three states of the suspension. The first state is free state. In the second state, the dimple is closed. In the

third state, the dimple is separated. The suction force generated by negative pressure slider is more significant than positive pressure slider and results in larger lift-up velocity of slider. The maximum velocity of the negative pressure slider without suspension limiters is 15.88 mm/s.

The flying height and velocity profiles during the dynamic unload of the negative pressure slider with suspension limiters are shown in Fig. 5.3 (c). With the limiters on the suspension, the unloading time is greatly shortened compared to negative pressure slider without suspension limiters. There are a total of four states of suspension. The first is free state. In the second state, the dimple is closed and limiters are open. In the third state, the dimple separates, and limiters are open. In the fourth state, the dimple separates and limiters are engaged [36]. The limiters prevent large dimple separation during unload, but the lift-off forces are increased. The negative pressure sliders are lifted up faster than positive pressure slider, and the negative pressure slider with suspension limiters is lifted up even faster than the negative pressure slider without suspension limiters. The maximum velocity of negative pressure slider with suspension limiters is 27.18 mm/s.

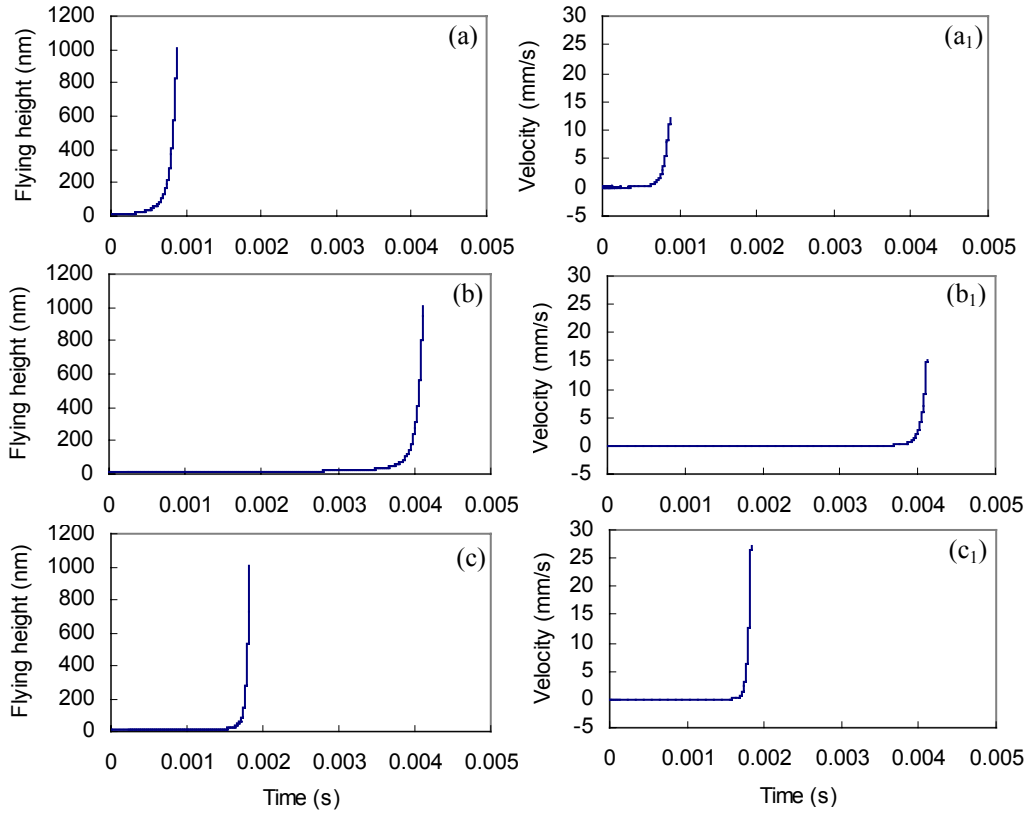


**Figure 5.3 Flying height and velocity performance of three sliders during dynamic unload (a) positive pressure slider (b) negative pressure slider without suspension limiters (c) negative pressure slider with suspension limiters**

Fig. 5.4 shows the calibration curves before and after passing through the photodetector of the three sliders during dynamic unload. After passing through the photodetector, the calibration curve may be distorted. The distortion means that the peaks and valleys are no longer being accurate. The corresponding results are shown in Table 5.1.

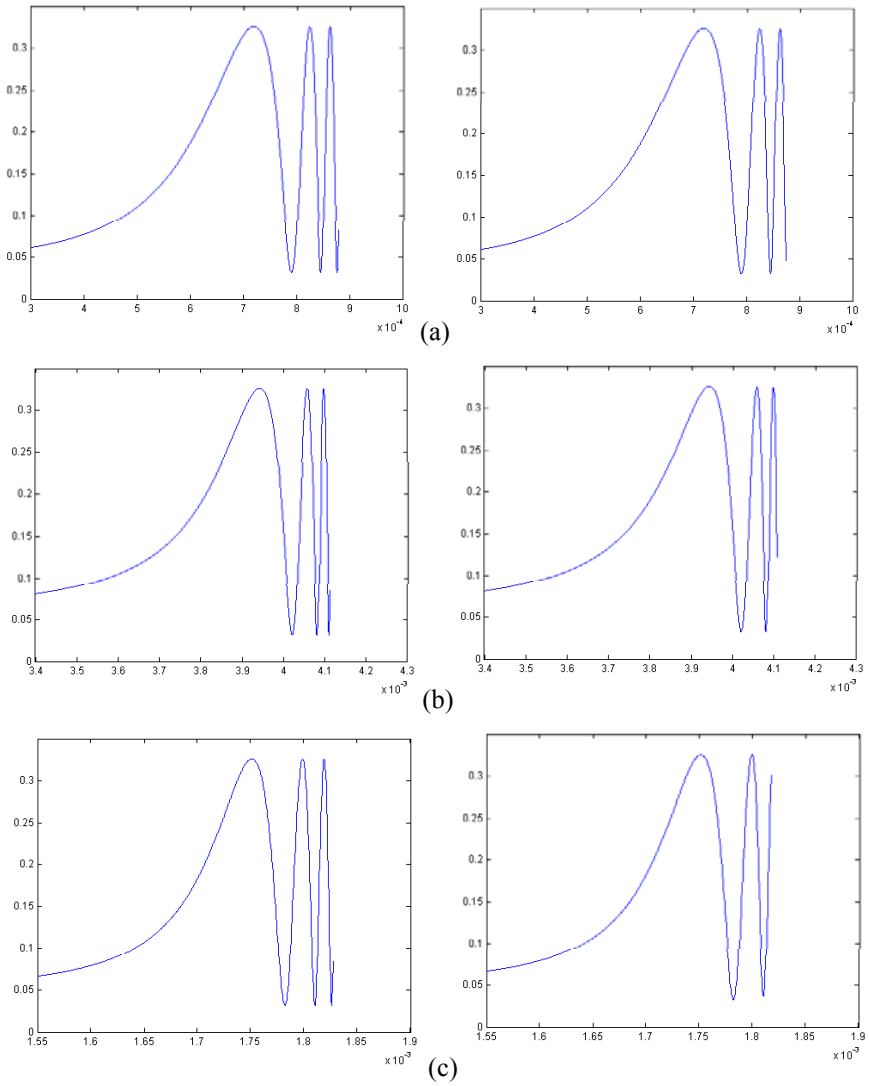


**Figure 5.4 Calibration curves before and after passing through the photodetector of three sliders during dynamic unload process (a) positive pressure slider (b) negative pressure slider without suspension limiters (c) negative pressure slider with limiters**

**Table 5. 1 Results in unloading process**

| | | $I_{max1}$ | $I_{min1}$ | $I_{p-p}$ | $FH_{error}$ |
|---|---|---|---|---|---|
| (a) | $I_{ideal}$ | 0.326373 | 0.031519 | 0.294854 | 0.16 nm |
| | $I_{actual}$ | 0.326354 | 0.031765 | 0.294589 | |
| | Difference | 0.000019 | 0.000246 | 0.000265 | |
| (b) | $I_{ideal}$ | 0.326373 | 0.031519 | 0.294854 | 0.31 nm |
| | $I_{actual}$ | 0.326329 | 0.031967 | 0.294362 | |
| | Difference | 0.000044 | 0.000448 | 0.000508 | |
| (c) | $I_{ideal}$ | 0.326351 | 0.031574 | 0.294776 | 0.35 nm |
| | $I_{actual}$ | 0.326119 | 0.032045 | 0.294074 | |
| | Difference | 0.000232 | 0.000471 | 0.000702 | |

*** (a) positive pressure slider, (b) negative pressure slider without suspension limiters and (c) negative pressure slider with suspension limiters**

From Table 5.1, it is observed that the error involved in the minimum intensity, $\Delta I_{min1}$, is different from the error involved in the maximum intensity, $\Delta I_{max1}$, and also the $\Delta I_{min1}$ is always larger than $\Delta I_{max1}$. This is because the vertical motion velocity of slider at $I_{min1}$ is always larger than that when the intensity reaches $I_{max1}$. Higher vertical motion velocity corresponds to more severe distortion caused by the frequency response of the photodetector. Hence, the minimum intensity is more possible to be distorted than the maximum intensity.

Comparing among the three sliders, the calibration error produced by negative pressure sliders during dynamic unloading are larger than positive pressure slider. The calibration errors produced by negative pressure slider with suspension limiters are even more significant than negative pressure slider without suspension limiters. The amount of error is determined by the amount of suction force produced in unloading process. The larger the suction force is, the faster the slider is lift-up. Comparing Fourier transform of the calibration curves of the three sliders, it can be found that the frequencies contained in the Fourier transform of calibration curve when using negative pressure slider with suspension limiters will concentrate at the higher

frequency region. That means there will be more frequency components in the region where $|H(jw)|$ begins to attenuate. From previous analysis, the calibration curve is therefore more desirable to be distorted. Therefore, the larger the velocity of slider, the more serious the calibration error obtained.

### 5.2.2 Loading Process Based Calibration

The accuracy of calibration and flying height measurement during dynamic load process is also investigated. The purpose is to see whether the calibration can be performed in loading process. Theoretically, there is no difference for calibration to be operated under either unloading process or loading process. However, if the effect of suction force, the velocity of slider and the frequency response of photodetector are considered, the difference appears.

The flying height and velocity profiles of the three types of sliders used for loading process calibration study are shown in Fig. 5.5. The flying height is at its range of 1000~0 nm. It is enough for the slider to complete calibration process.

The flying height and corresponding velocity profiles in loading process of positive pressure slider are shown in Fig. 5.5 (a). It can be found that the flying height profile is not smooth with amplitude flying height oscillation. In such a loading process, the maximum speed of the slider is 30.23 mm/s.

The flying height and corresponding velocity performances in loading process of negative pressure slider without suspension limiters are shown in Fig. 5.5 (b). The loading process is not very smooth without head disk contact. Flying height amplitude can also be seen when slider approaches disk if that portion is amplified. The maximum velocity of slider in this loading process reaches 38.12 mm/s.

Fig. 5.5 (c) displays the flying height and velocity profiles during dynamic load process of negative pressure slider with suspension limiters. The slider reaches its maximum velocity of 40.97 mm/s.

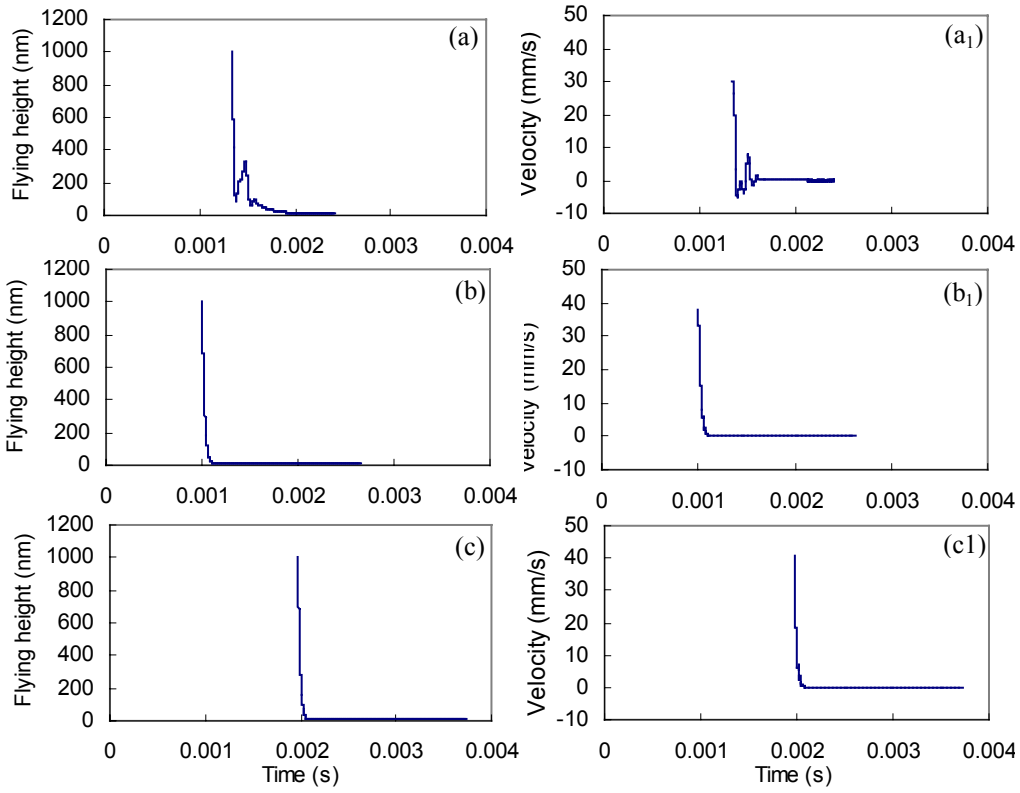


**Figure 5.5 Flying height velocity performance of three sliders during loading process (a) positive pressure slider (b) negative pressure slider without suspension limiter (c) negative pressure slider with suspension limiter**

Fig. 5.6 shows the calibration curves before and after passing through the photodetector of the three sliders during loading process. Because the positive pressure slider bounces several times before it is fully loaded, the calibration curve is not so smooth. For the other two negative pressure sliders, the calibration curves are smoother. The corresponding results are shown in Table 5.2.

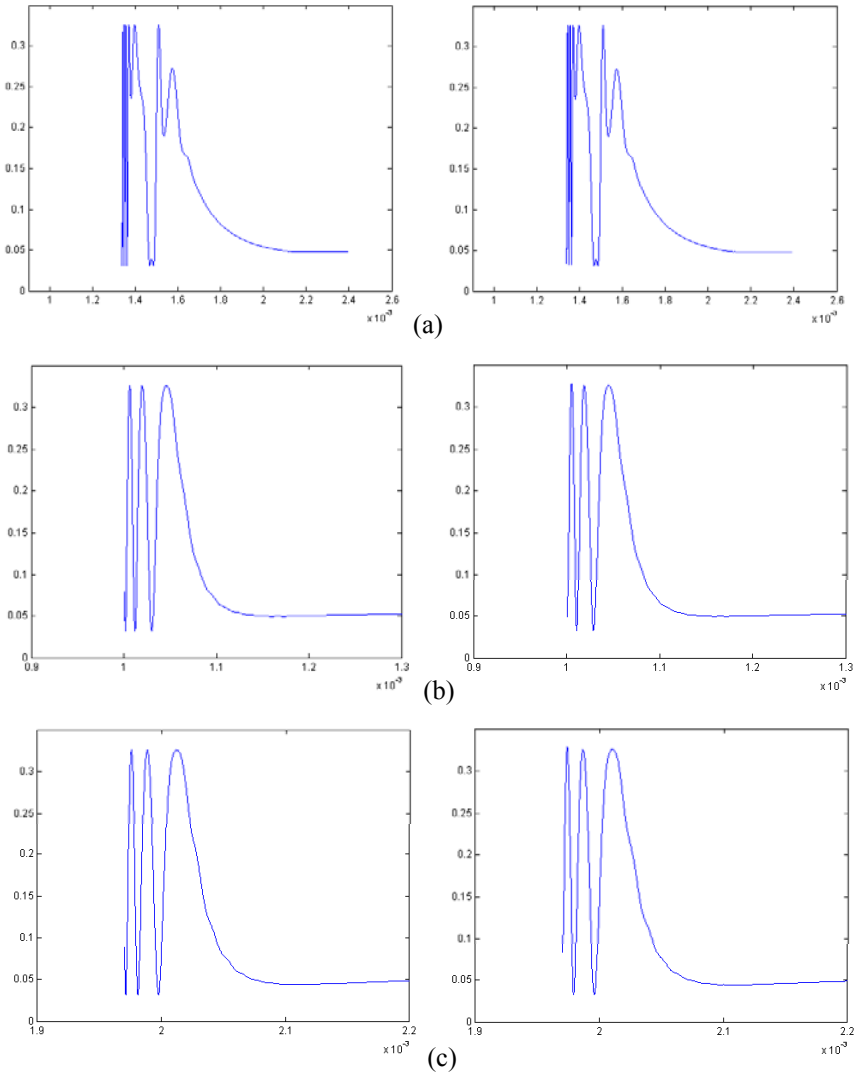


**Figure 5.6 Calibration curves before and after passing through the photodetector of three sliders during dynamic load process (a) positive pressure slider (b) negative pressure slider without suspension limiters (c) negative pressure slider with limiters**

**Table 5. 2 Results in loading process**

| | | $I_{max1}$ | $I_{min1}$ | $I_{p-p}$ | $FH_{error}$ |
|---|---|---|---|---|---|
| (a) | $I_{ideal}$ | 0.326341 | 0.031518 | 0.294824 | 0.21nm |
| | $I_{actual}$ | 0.326309 | 0.031553 | 0.294757 | |
| | Difference | 0.000032 | 0.000035 | 0.000067 | |
| (b) | $I_{ideal}$ | 0.326371 | 0.031522 | 0.294849 | 0.47nm |
| | $I_{actual}$ | 0.326147 | 0.032214 | 0.293933 | |
| | Difference | 0.000224 | 0.000692 | 0.000916 | |
| (c) | $I_{ideal}$ | 0.326372 | 0.031518 | 0.294855 | 0.49nm |
| | $I_{actual}$ | 0.326086 | 0.032239 | 0.293847 | |
| | Difference | 0.000286 | 0.000721 | 0.001008 | |

***(a) positive pressure slider, (b) negative pressure slider without suspension limiters and (c) negative pressure slider with suspension limiters**

The same trend as the unloading process can be obtained from loading process. The error involved in minimum intensity is always larger than the error involved in maximum intensity. Meanwhile, the calibration error and flying height measurement error are the most significant when using negative pressure slider with suspension limiters during dynamic loading process. However, there is no much difference for using negative pressure sliders between with and without suspension limiters. This is because the limiters do not operate in the loading process.

The flying height measurement error is more significant when calibration is performed based on loading process than unloading process. This is because for all the three sliders, the velocity of sliders during loading process is larger than unloading process.

### 5.2.3 Effects of Loading/Unloading Vertical Velocity and Light Wavelength

The aim of this study is to understand whether changing loading/unloading speed could improve the calibration accuracy in flying height measurement.

Referring to negative pressure slider with suspension limiters, the flying height measurement errors during unload process at the vertical unloading velocities of 8 mm/s, 10 mm/s, 15 mm/s, and 20 mm/s are revealed in Fig. 5.7 (a).

It can be seen that the flying height measurement error increases as the loading/unloading vertical velocity increases. This is mainly associated with the amount of lift-off force generated in unloading process. The lift-off force is a function of vertical unloading velocity. A smaller velocity gives a smaller lift-off force because of smaller squeeze effects of the air bearing and therefore results in smaller flying height measurement error [37]. From Fig. 5.7 (a), it is known that the bandwidth of photodetector should be set at least 108 kHz in order to keep flying height error below 0.1nm.

Fig. 5.7 (b) displays the flying height measurement error during dynamic unload process at different light wavelengths of 450 nm, 550 nm, and 650 nm. The flying height measurement error is the largest when using 650 nm wavelength and is the smallest when using 450 nm wavelength. This is because more frequency components in Fourier transform of calibration curve with 650 nm wavelength fall in the region where the magnitude of the transfer function of photodetector begins to attenuate. Therefore, it results in larger calibration error and flying height measurement error.

To keep the error below 0.1 nm, the bandwidth of photodetector should be larger than 110kHz, 120kHz, and 130kHz when using 450 nm, 550 nm, and 650 nm wavelength respectively.

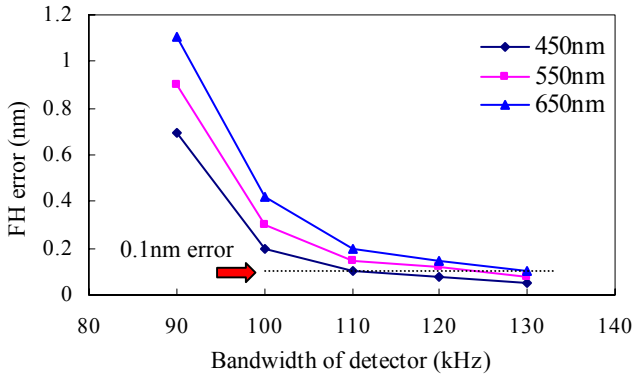


**(a)**

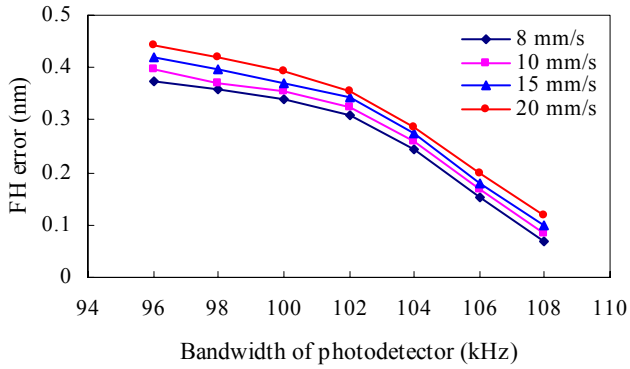


**(b)**

**Figure 5.7 Flying height error caused under different condition (a) Wavelength impact on FH measurement error (b) L/UL velocity impact on FH measurement error**

# 5.3 Error Compensation

## 5.3.1 Compensation Method

A filter that does not distort signals will have a response that is equal to a constant which covers all frequency components of the Fourier transform of the flying height variation in calibration process. The ideal case is that the photodetector has an infinite high cut-off frequency or bandwidth which won't cause any signal distortion.

For calibration, the most critical issue is the accuracy of maximum and minimum intensities. The fundamental solution idea is to push cut-off frequency higher so as to make more frequency components present in Fourier transform of calibration curve

concentrating at a region where the magnitude of pass band is equal to one. To realize this object, it is required for a compensator that can be appended in a cascade arrangement following the photodetector, as shown in Fig. 5.8. It is assumed that the frequency response of the photodetector is $H_1(jw)$, and the frequency response of the compensator is $H_2(jw)$.

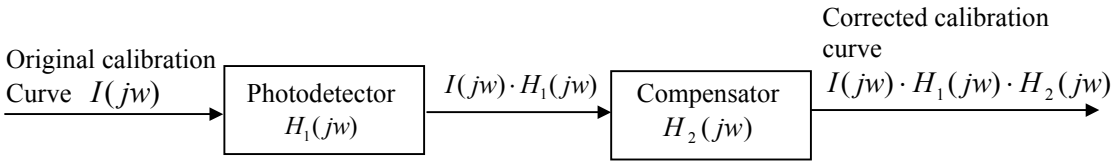


**Figure 5.8 Compensation method**

The frequency responses of the photodetector and compensator are shown in Fig. 5.9. Actually the $H_2(jw)$ is the inverse of $H_1(jw)$, such that $H_2(jw)=1/H_1(jw)$. This can be achieved by using some suitable frequency transformations. Note that if the value of $H_1(jw)$ is $|H_1(jw)|e^{j\phi}$, the value of $H_2(jw)$ is $\frac{1}{|H_1(jw)|}e^{-j\phi}$. However, if $|H_1(jw)|$ is too small and approaching rejection band, $|H_2(jw)|$ will be quite large in that region. This is unacceptable. Therefore, a proper compensation scheme is to compensate up to cut-off frequency only. Therefore, a proposed compensation function is:

$$H_2(jw)=1/H_1(jw); \qquad 0\le w<w_c \tag{5.15a}$$

$$H_2(jw)=cons\tan t; \qquad w_c\le w<w_r \tag{5.15b}$$

$$H_2(jw)=0; \qquad w_r\le w<\infty \tag{5.15c}$$

The compensator compensates frequency response to constant for frequency up to cut-off frequency. Then, it provides certain level of compensation from the frequency between cut-off frequency and rejection frequency, aiming to have a smooth transition from the fully compensated status to no compensation status. Therefore, the compensation scheme is called cut-off frequency compensation.

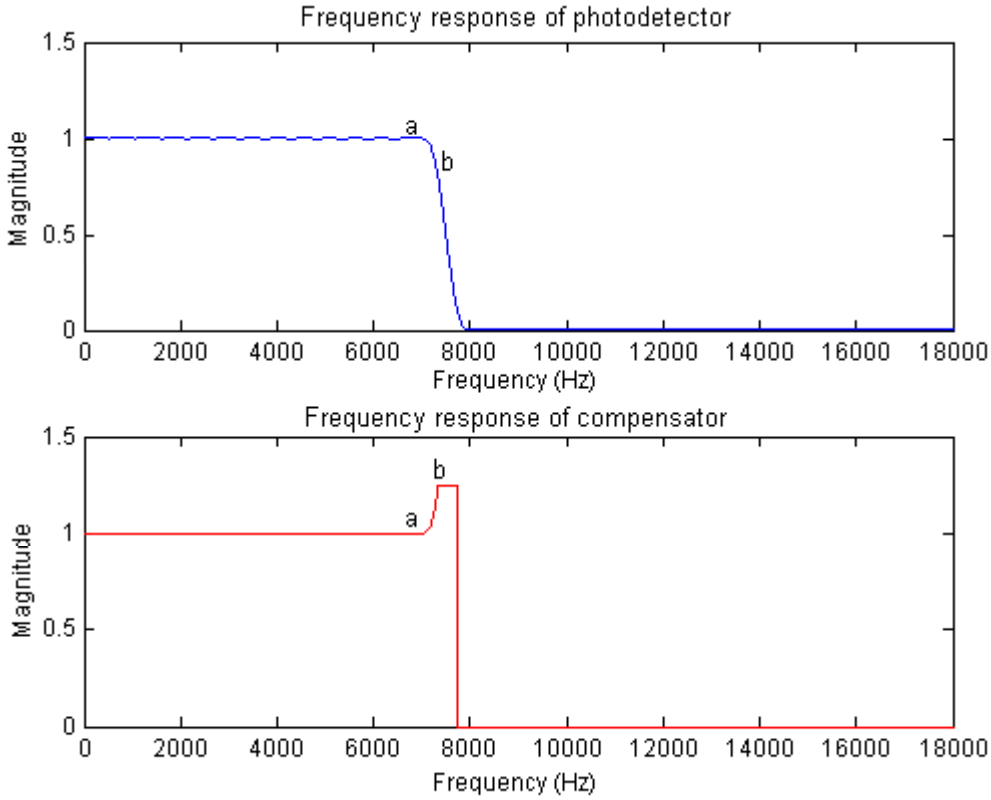


**Figure 5.9 Frequency response of photodetector and compensator**

The $|H_2(jw)|$ is shown in bottom plot of Fig. 5.9. After compensation, the error in maximum and minimum intensities of original calibration curve can be reduced. In frequency response of photodetector, from a to b, the magnitude is declined, but in the frequency response of compensator, the magnitude is inclined from a to b. So, the pass band is widened, and thus theoretically the error compensation is realizable.

### 5.3.2 Compensation Realization

The purpose of this section is to verify the feasibility of the above-mentioned error compensation method and further investigate how much flying height can be corrected by using the above method. First, a flying height was tested with the state-of-the-art flying height tester. The slider used was pico negative pressure slider. Both the calibration trace and measurement trace were performed at 7200 rpm, 30 mm radius and zero skew angle. The reported flying height by the flying height tester was 11.08 nm. During the testing, the raw data of both calibration trace and measurement trace are recorded. Then with Matlab program, the calibration curve is imported into the compensator mentioned above. After passing through the compensator, it is found that the peak-to-peak value is enlarged. This means the maximum and minimum intensities are detected more accurately and in turn, the flying height is corrected by 0.183 nm.

Since there are some noises on the calibration curve, it is not easy to determine which intensity value is the maximum and which is the minimum. Therefore, the curve fitting technique is used to find out the extremum. Fig. 5.10 shows the calibration curves. The top figure shows the original calibration curve and the bottom figure shows the calibration curve dealing with curve fitting. The results after cut-off compensation are shown in Table 5.3. From the Table 5.3, comparing with original calibration curve, in the corrected calibration curve, the maximum intensity increases by 1.2 count, the minimum intensity decreases by 2.63 count and the peak-to-peak value increases by 3.83 count. Using the same measurement trace, the flying heights obtained are 11.018nm and 11.2nm based on actual and corrected calibration curve respectively. The corrected one is 0.183nm. This demonstrates that this compensation scheme works.

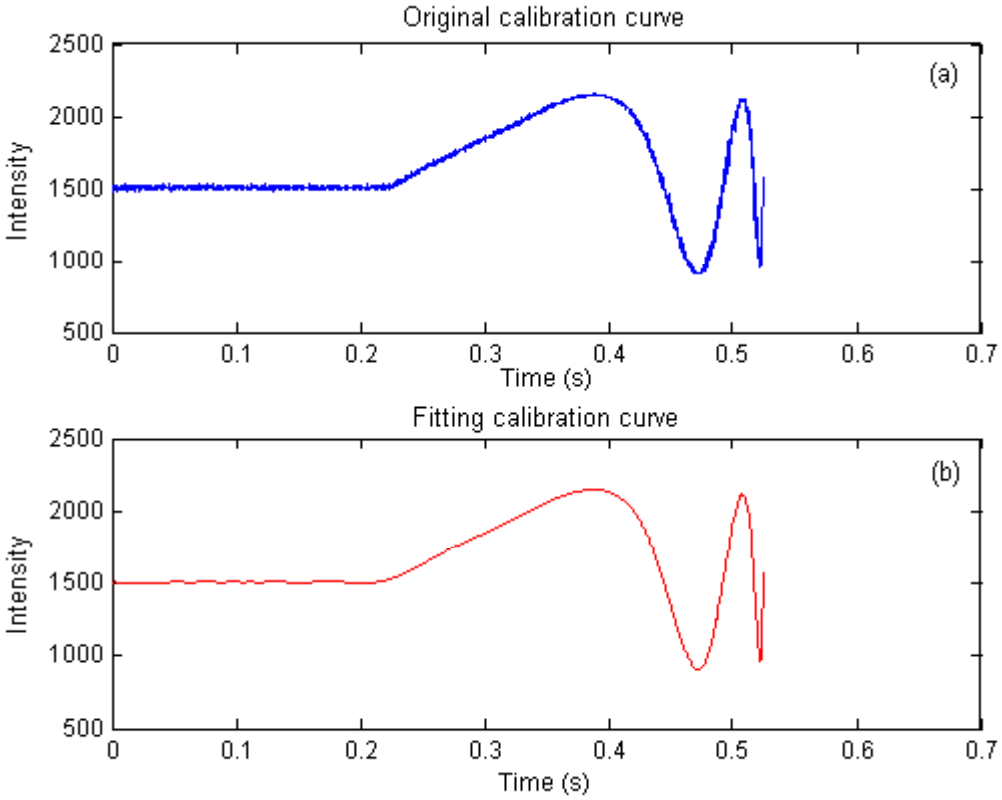


**Figure 5. 10 Calibration curves (a) original calibration curve (b) fitting calibration curve**

**Table 5. 3 Comparison of actual and corrected calibration curves**

| | Maximum intensity | Minimum intensity | P-p value | Flying height (nm) |
|---|---|---|---|---|
| Original calibration curve | 2148 | 906.9 | 1241.1 | 11.018 |
| Corrected calibration curve | 2149.2 | 904.3 | 1244.9 | 11.201 |
| Difference | 1.2 | 2.6 | 3.8 | 0.183 |

## 5.4 Summary

In this chapter, the combined effect of both strong suction force of negative pressure sliders and limited cut-off frequency of photodetector is further investigated. Both positive pressure slider and negative pressure slider with and without suspension limiters are included in the analysis.

For unloading based calibration, negative pressure slider with suspension limiter gives largest calibration error and flying height measurement error. Loading process is not suitable for flying height calibration as the loading process always generates larger calibration error, comparing with unload process based calibration. Reduced unloading velocity helps the reduction of calibration error and flying height testing error. A cut-off frequency compensation scheme is proposed. Results indicate that the method can effectively improve the calibration accuracy.

# Chapter 6

# Light Spectrum, Optical Filter and Flying Height Measurement Accuracy

## 6.1 Introduction

From chapter 2, it is known that the three-wavelength interferometry, the standard flying height testing technology, will remain as the only mainstream choice of slider's flying height test.

The light source is of wide spectrum. In order to select three distinct wavelengths, there will be an optical filter placed in the optical path of each optical beam to transmit light at the chosen wavelength with a specified width [11].

Optical filters, especially optical interference filters, are one of the most important optical components of the flying height testing system [38]. In optical interference filters, wavelength selection is based on the property of destructive light interference. Incident light passes through two coated reflecting surfaces. In situations where the reflected beams are in phase, the light will pass through the two reflective surfaces. However, if the wavelengths are out of phase, destructive interference will block most of the reflections, allowing almost nothing to transmit through. In this way, optical interference filters are able to attenuate the intensity at undesired wavelengths. The spectral characteristic of optical interference filters is shown in Fig. 6.1.

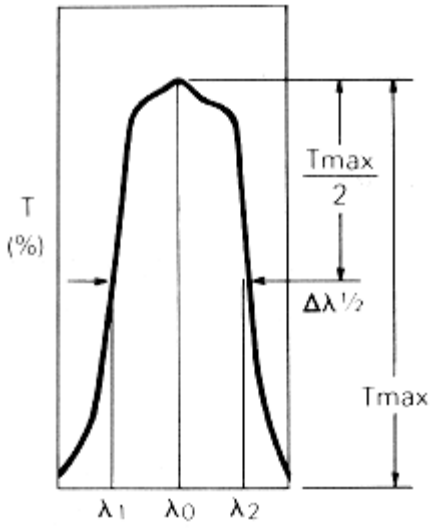


T(%): transmittance
$T_{max}$: maximum transmittance
$\lambda_0$: center wavelength
$\Delta\lambda^{1/2}$: half-width
$\lambda_1$: starting wavelength
$\lambda_2$: ending wavelength
$\lambda_0=(\lambda_1+\lambda_2)/2$

**Figure 6.1 Spectral characteristic of interference filter**

The optical filters typically permit 10% to 70% light transmission. The transmission is defined as the ratio of light transmitted through the optical filter to the light incident on the optical filter. The center wavelength is specified at which the maximum transmission occurs. The half-width $\Delta\lambda^{1/2}$ of the optical filter is the difference between the wavelengths at which the transmittance is a half of transmission. Referring to Fig. 6.1, the distance between the two wavelengths $\lambda_1$ and $\lambda_2$ is called the bandwidth of the optical filter. In fact, it is impossible to just select one frequency while filter out the rest spectrums.

Currently, the industry standard flying height testers use the response of center wavelength $\lambda_0$ of the optical filter to fully represent the optical performance of the light beam after the optical filter. However, no literature has studied whether such an approximation could cause any errors in flying height testing.

This chapter investigates what is the best way of handling the light beam after an optical filter which is of non zero half-width $\Delta\lambda^{1/2}$.

## 6.2 Light Source and its Spectrum

### 6.2.1 Super-High Pressure Mercury Lamp

The super-high pressure Mercury lamp was used as the light source of the first few generations of three-wavelength optical interferometry.

Fig. 6.2 (a) shows the spectrum distribution of this lamp. It displays the relative light output from 0 to 100%. The output spectrum of the lamp is dominated by strong mercury lines in visible and ultraviolet region. It can be seen that there are strong peaks at 436 nm, 546 nm and 577 nm. For the rest of the useful wavelength range, the emission is rather steady but not intense enough. This is also its particular disadvantage. The individual lines can be isolated using filters. Narrowband optical filter with a bandwidth of 10 nm is used to select the wavelength at 436 nm, 546 nm and 580 nm.

### 6.2.2 Super-Quiet Xenon Lamp

Due to the shortcomings of mercury lamp, super-quiet Xenon lamp is utilized as light source for the state-of-the art flying height testers. It is of high radiant and more evenly throughout over a wide spectrum of light wavelength. It emits a continuous spectrum of light ranging from ultraviolet to visible and infra-red. Some lines spectra are radiated in the visible light range and conspicuous line spectra in the infra-red light range as shown in Fig. 6.2 (b). Because of this reason, the optical filter used is of wider half-width $\Delta\lambda^{1/2}$, aiming to pursuing stronger intensity and higher signal-to-noise ratio (SNR) which are required in optical systems. Currently, in the industry standard flying height tester, the optical filter with a bandwidth of 40 nm is utilized.

For example, the filter for 650 nm center wavelength, it may transmit light from 630 nm to 670 nm.

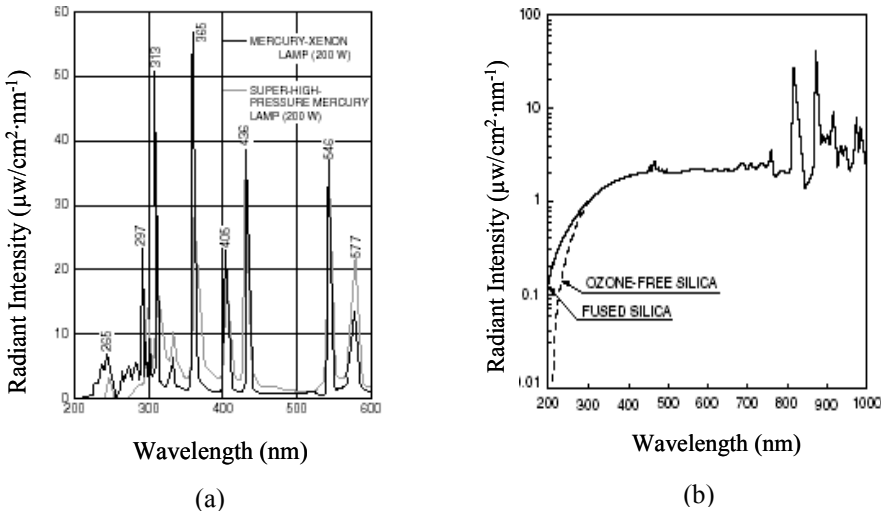


**Figure 6.2 Spectral distribution of light source**

**(a) Super-quiet mercury lamp emission spectrum (b) Super-quiet Xenon lamp emission spectrum**

## 6.3 Calibration Error Caused by Optical Filter

Following analysis will exhibit that using broaden bandwidth optical filters in optical flying height testing system can cause a calibration error. This is a systematic error which will result in flying height measurement error.

Up to now, all the analyses in public domain assume that the light after optical filter is a single wavelength. Nevertheless, this is not true in practice. Real situation is that the light received by a photodetector is not monochromatic and of a spectrum over a range of wavelength. The extra interference that comes from the extra frequency content in the signal will lower the level of signal peaks and also raise the signal valleys, resulting in diminished peak-to-valley values. This phenomenon is called calibration falloff, as shown in Fig. 6.3. The errors produced in the maximum and minimum intensities of calibration when using optical filters with bandwidths of 20 nm, 40 nm and 80 nm are displayed in Table 6.1.

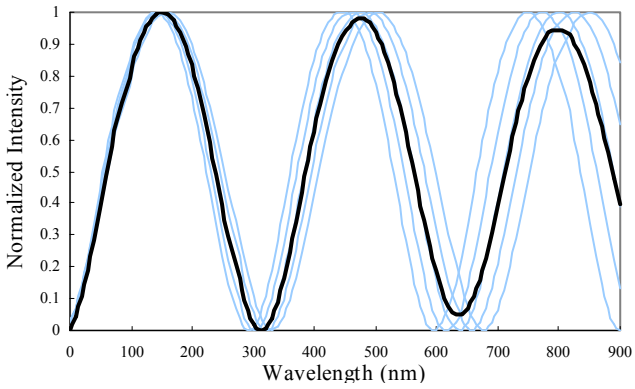


**Figure 6.3 Calibration falloff caused by optical filter bandwidth**

**Table 6. 1 Calibration errors caused by optical filter**

| Bandwidth | $I_{max}$ | $I_{min}$ | Peak-to-valley |
|---|---|---|---|
| 0 nm | 0.31984 | 0.04781 | 0.27203 |
| 20 nm | 0.31981 | 0.04808 | 0.27173 |
| 40 nm | 0.31972 | 0.04891 | 0.27081 |
| 80 nm | 0.31933 | 0.05212 | 0.26721 |

Here, zero half-width $\Delta\lambda^{1/2}$ is the ideal case and can be used as a reference. From Table 6.1, it is observed that as the bandwidth of optical filter increases, the magnitude of maximum intensity decreases, the level of minimum intensity raises and moreover the peak-to-valley value reduces. This means that the wider the bandwidth of optical filter, the more serious the calibration falloff. This will cause serious flying height measurement error which can not be ignored. The calibration falloff is unavoidable. We must find a way to eliminate such error.

## 6.4 Equivalent Wavelength of Optical Filter

Since light is not monochromatic and the light passing through the optical filter is still with a wavelength band. In the flying height measurement and calculation, it is the most accurate if considering the total input energy received by the photodetector. The total energy is the integral of the power distribution of light source. During the

calculation, we get an accurate calibration curve which is of falloff characteristic. From this curve, an equivalent wavelength can be obtained using some specified method. However, when the equivalent wavelength is used to get the calibration curve, it is found that this curve is always different from the accurate curve, because this curve is not of falloff characteristic. There is error involved in the maximum and minimum intensities of calibration curve. To further improve the flying height measurement accuracy, it is necessary to find a way to eliminate such error.

The method to get the equivalent wavelength and minimize the calibration error is described below:

$$I_s = I_0 \frac{r_{20}^2 + |r_{01}|^2 + 2r_{20}|r_{01}|\cos(\delta + \phi_s)}{1 + r_{20}^2|r_{01}|^2 + 2r_{20}|r_{01}|\cos(\delta + \phi_s)} \tag{6.1}$$

where, $\delta = \frac{4\pi h}{\lambda}$, $\phi_s = \pi - \tan^{-1}(\frac{2n_0k_1}{n_0^2 - n_1^2 - k_1^2})$, $r_{20} = \frac{n_2 - n_0}{n_2 + n_0}$, $r_{01} = \frac{n_0 - (n_1 + ik_1)}{n_0 + (n_1 + ik_1)}$, h is the flying height and λ is the light wavelength. $I_0$ is the input light intensity and $I_s$ is the output light intensity.

Generally, the input light intensity is assumed to be 100% without any losses. However, due to the different spectral responses of light source, optical filter and photodetector, the transmittance of input light intensity is not uniform over the wavelength band. Therefore, $I_{in}$ becomes a function of wavelength.

Fig. 6.4 (a) shows the tested spectrum distribution of the Xenon lamp. Figures 6.4 (b) to (d) demonstrate the spectral characteristics of the optical filters with bandwidths of 20 nm, 40 nm and 80 nm. The spectral characteristics of optical filters are characterized by the light transmission. The spectral response of photodetector is displayed in Fig. 6.4 (e). The photodetector used in the optical flying height testing system is of the advantages of high sensitivity and high speed. Its spectral response

occurs from 400 nm to 1000 nm. The spectral response of a photodetector is described by absolute responsivity in units of amperes/watt (A/W).

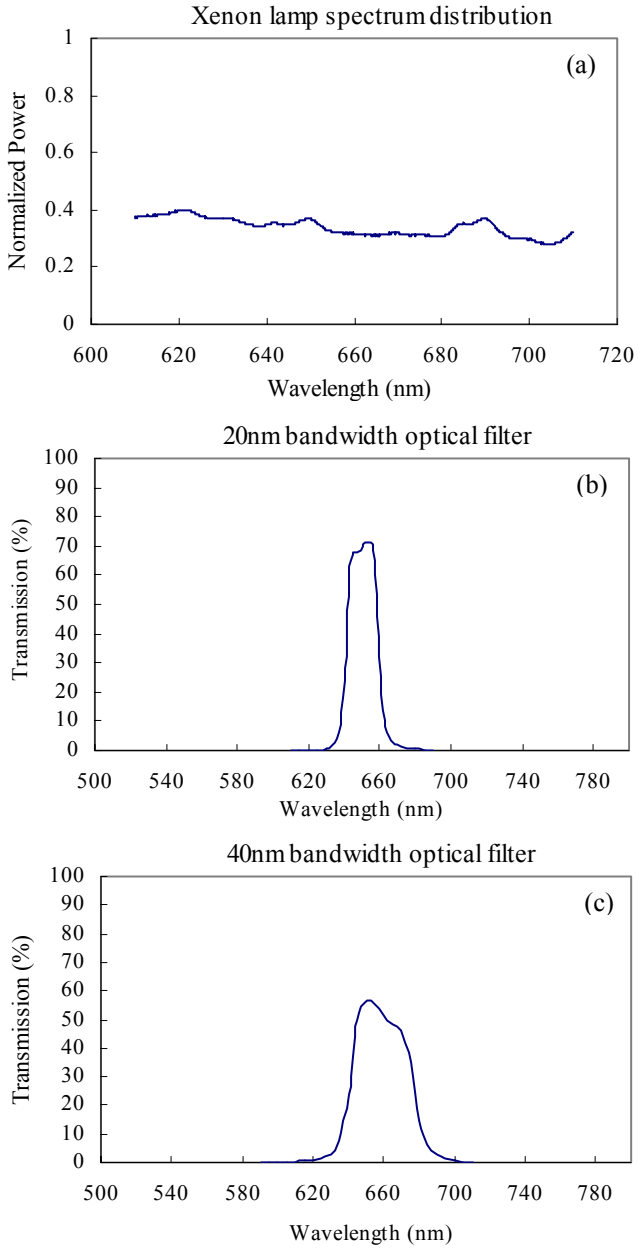

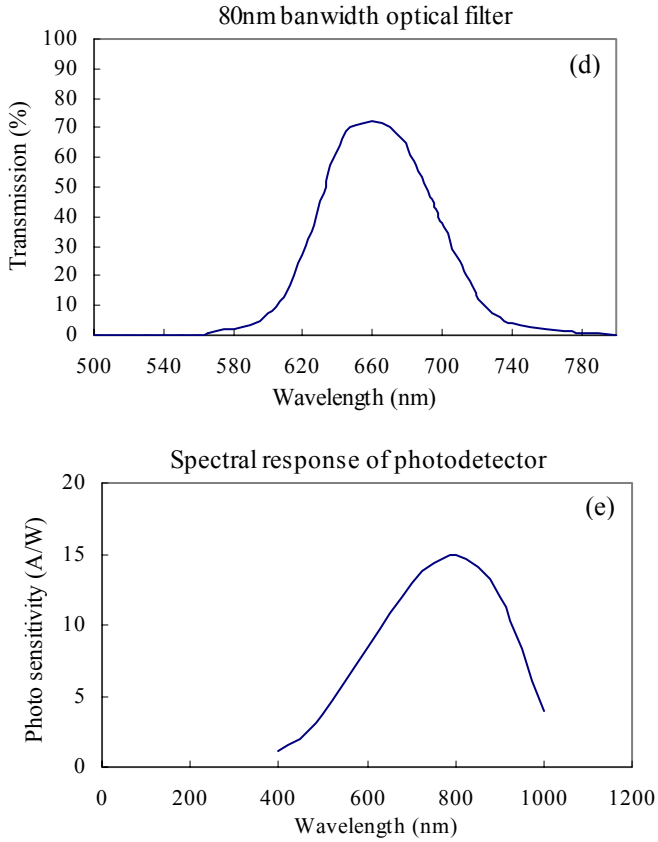


**Figure 6.4 Spectral characteristics of light source, optical filters and photodetector**

The equivalent wavelength for a combination of, for instance, light source, photodetector and an optical filter with a center wavelength of 650 nm and a bandwidth of 40 nm can be obtained in such a way:

1) To find the total spectral transmittance of the light source, photodetector and optical filter by multiplying the spectral transmittance of each component, as shown in Fig. 6.5 (a). The relationship between $I_{in}$ and λ is obtained.

2) For each light wavelength from 641.1 nm to 676.8 nm, a group of intensity vs. flying height curves can be plotted under the condition of $I_{in}$ is a function of λ, as demonstrated in Fig. 6.5 (b).

3) The group of curves are summed, averaged and then normalized to get a new theoretical intensity vs. flying height curve, which is displayed in Fig. 6.5 (c).

4) To find the corresponding spacing where the maximum and minimum intensities occur.

As is well known, the distance between the two adjacent peaks and valleys is equivalent to λ/4, such as $\Delta FH = \frac{\lambda_e}{4}$. This relationship enables us to convert the distance, $\Delta FH$, into equivalent wavelength, $\lambda_e$. The results are shown in Table 6.2.

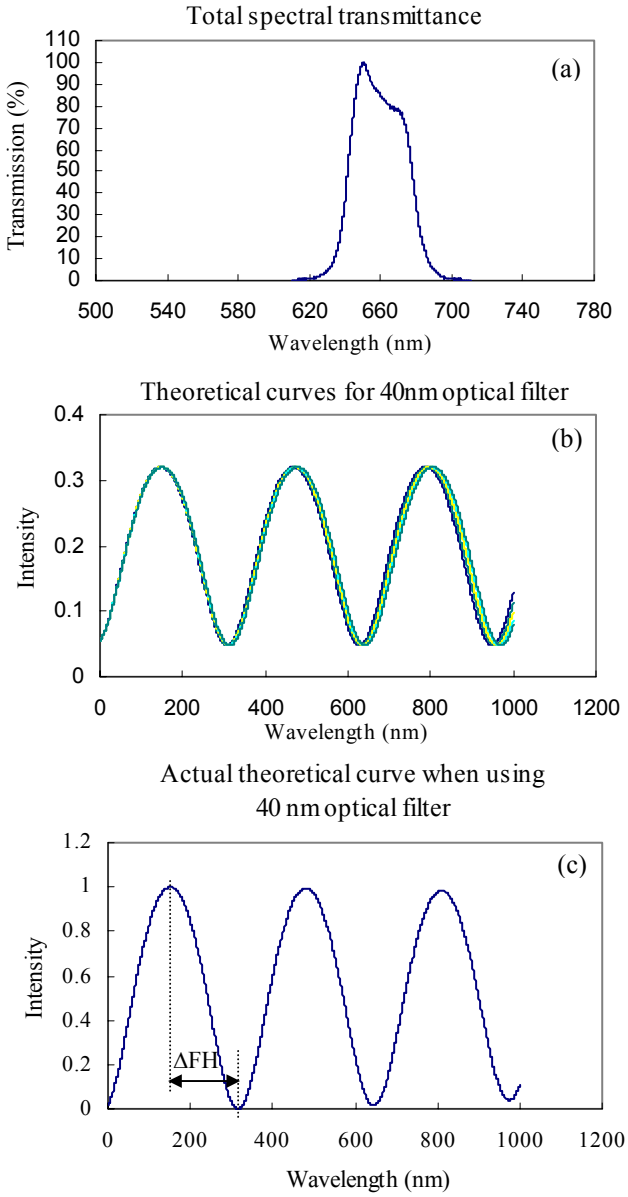


**Figure 6.5 Process to get equivalent wavelength**

**Table 6. 2 Equivalent wavelengths**

| | FH at $I_{max}$ | FH at $I_{min}$ | ΔFH | Equivalent wavelength |
|---|---|---|---|---|
| 20 nm | 149.3 nm | 312 nm | 162.7 nm | 650.8 nm |
| 40 nm | 151.1 nm | 315.8 nm | 164.7 nm | 658.8 nm |
| 80 nm | 151.9 nm | 317.5 nm | 165.6 nm | 662.4 nm |

The actual theoretical curves when using optical filters with bandwidths of 20 nm, 40 nm and 80 nm are shown in Fig. 6.6. It can be observed that these curves have the falloff characteristics. If we use these curves as theoretical curve when calculating flying height, the calibration error mentioned in section 6.2 can be eliminated. In other words, the proposed calibration process is to use the integral response curve as illustrated in Fig. 6.5 (c) as the theoretical curve for flying height measurement. As the curve is obtained by integration of interference over whole spectrum of light source, it is referred to it as "integral response method" in this thesis.

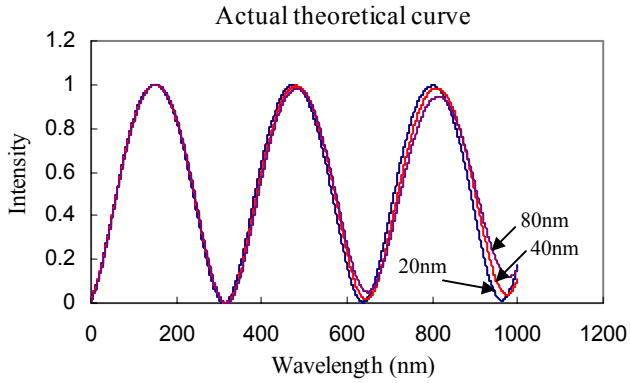


**Figure 6.6 Actual theoretical curves when using optical filters with bandwidths of 20 nm, 40 nm and 80 nm**

## 6.5 Experiment

The broad bandwidth of optical filter is usually deemed as a drawback because it causes serious calibration error. However, this error can be eliminated by using a new theoretical curve which is obtained from the integral response method. The new

theoretical curve is obtained after considering the effect of spectral characteristics of light source, optical filter and photodetector. Here, instead of treating the broad bandwidth of optical filter as a disadvantage, a serious of experiments are performed to investigate whether we can make use of broadband optical filters to improve signal quality and further improve the repeatability of flying height measurement.

Three optical filters with bandwidths of 20 nm, 40 nm and 80 nm are used in the experiment.

### 6.5.1 Signal Quality

The signal-to-noise ratio is an important factor to determine whether the signal quality is better or not.

The signal quality analysis is based on light intensity signal obtained in the calibration process. In the calibration curve, the magnitude of peak-to-valley value of interference intensity is defined as signal level. The magnitude of peak-to-peak value of interference intensity at a fixed flying height is defined as noise level. The noise comes most likely from background light, thermal effect, electronics noise, and air disturbances.

### 6.5.2 Repeatability of Flying Height Measurement

The purpose of this experiment is to investigate whether the repeatability of flying height measurement can be improved by using optical filters with broader bandwidth. In order to focus on the influence of optical filters, the slider with a flying height of 38 nm is used in this experiment. Firstly, the optical filter with a bandwidth of 20 nm is installed on the 650 nm channel of the flying height tester. The dynamic loading/unloading calibration is repeated 15 times. Then the optical filter with a

bandwidth of 40 nm is exchanged on the 650 nm channel without altering any other things. After 15 times of loading/unloading operation, the optical filter with a bandwidth of 80 nm is exchanged.

## 6.6 Experiment Results and Discussion

### 6.6.1 Signal Quality

The calibration curves using the three optical filters are shown in Fig. 6.7. It is found that the magnitude of signal level increases as the bandwidth of optical filter increases. Especially, the magnitude of signal level is greatly improved when using the optical filter with a bandwidth of 80 nm. On the other hand, the magnitude of noise level also increases when the bandwidth of optical filter is increased. Currently, the optical filters with a bandwidth of 40 nm are used in the state-of-the-art flying height tester. It is believed that the SNR of the system can be further improved by using the optical filters with a bandwidth of 80 nm and the new theoretical curve defined by the integral response method.

The results are shown in Table 6.3.

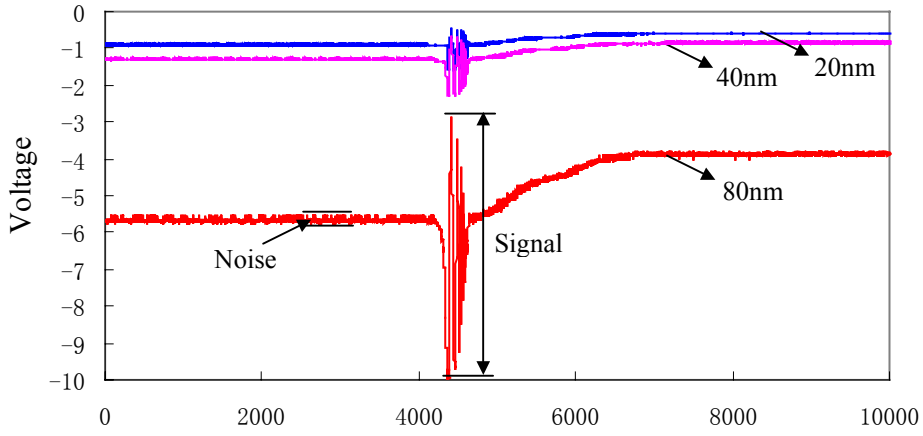


**Figure 6.7 Calibration curves performed when disk in held in stationary state**

**Table 6. 3 SNR of optical filters with bandwidths of 20 nm, 40 nm and 80 nm**

| Bandwidth | 20 nm filter | 40 nm filter | 80 nm filter |
|---|---|---|---|
| Signal | 1.14062 | 1.6919 | 7.125 |
| Noise | 0.04688 | 0.04789 | 0.125 |
| SNR | 24.33 | 35.329 | 57 |

### 6.6.2 Testing Accuracy and Repeatability

When calculating flying height, the integral response method and the new theoretical curves are used to eliminate the error caused by calibration falloff. The measurement results are shown in Table 6.4. It can be found that after error compensation, comparing the averaged flying height measured when using optical filters with bandwidths of 20 nm, 40 nm and 80 nm, the flying heights are kept at 38.4 nm with 0.05 nm fluctuation. The repeatability of using the optical filter with a bandwidth of 80 nm is better than the other two arrangements. This is mainly because the maximum and minimum intensities of calibration curve are detected more accurately. The SNR has a greatly important relationship with flying height measurement repeatability. Higher SNR means higher sensitivity and therefore better measurement repeatability.

## 6.7 Summary

Optical filter is a very important component of flying height testing system. The wider the half width of optical filter, the more severe the falloff of the calibration curve and the bigger the calibration error.

Such calibration error can be eliminated by the proposed integral response method and the new theoretical curve. The method and new calibration curve take into account of the spectral characteristics of light source, optical filter and photodetector.

Furthermore, the integral response method and the new calibration curve allow the use of wider bandwidth optical filter to increase the signal quality in flying height measurement.

Experiment results show that the stronger intensity of testing signal and better testing accuracy can be achieved by using broader bandwidth optical filters and the new theoretic curve.

**Table 6. 4 Testing repeatability when using three optical filters**

| | FH (nm) (20 nm filter) | FH (nm) (40 nm filter) | FH (nm) (80 nm filter) |
|---|---|---|---|
| 1 | 35.86 | 36.03 | 38.64 |
| 2 | 37.82 | 37.02 | 38.35 |
| 3 | 35.49 | 37.10 | 37.09 |
| 4 | 37.72 | 37.45 | 37.29 |
| 5 | 37.36 | 37.67 | 37.39 |
| 6 | 37.83 | 39.26 | 38.46 |
| 7 | 38.83 | 39.25 | 38.59 |
| 8 | 38.88 | 39.15 | 38.77 |
| 9 | 39.48 | 39.21 | 38.54 |
| 10 | 39.61 | 39.08 | 39.38 |
| 11 | 39.78 | 39.27 | 38.45 |
| 12 | 39.73 | 39.27 | 38.97 |
| 13 | 39.40 | 38.89 | 38.41 |
| 14 | 39.66 | 39.19 | 39.26 |
| 15 | 39.42 | 39.08 | 39.06 |
| Average | 38.458 | 38.4007 | 38.44333 |
| σ | 1.352076 | 1.050679 | 0.66631 |

# Chapter 7

# Conclusions

The research and development efforts of hard disk drives will continue to be aimed at achieving higher areal density by the continuing reduction of the head-disk spacing, or flying height. Currently technology allows for 8~10 nm head disk spacing in high-end commercial disk drives. As the areal density approaches 1 $Tb/in^2$, the head-disk spacing is projected to be below 3 nm. In such a low flying height region, it becomes more and more important, necessary but difficult to achieve high accuracy flying height measurement. In the flying height measurement, proper and accurate calibration is a severe challenge.

Two factors affecting the accuracy of calibration are investigated: cut-off frequency effect of the photodetectors used for flying height testing and the effect of optical filter bandwidth.

A detailed review and analysis of possible quantitative flying height testing technologies for flying height measurement in future hard disk drive manufacturing conclude that the three-wavelength intensity interferometry is still the most mature and promising technology for current and recent futures.

A modeling platform has been developed to understand and evaluate the calibration error and flying height measurement error of the three-wavelength intensity interferometry.

The results from the modeling platform suggest that the calibration error and flying height measurement error be more significant when the cut-off frequency of the photodetector is not high enough (not easy to have a photodetector of both high cut-

off frequency and high signal quality). On the other hand, the narrower bandwidth of optical filter causes comparatively smaller error on calibration and flying height measurement.

Systematic experiment studies were performed to investigate the limitations of current calibration method especially for sliders with strong negative pressure, as such sliders represent the future of slider technology. Results from experiment and modeling indicate that one concern in future flying height measurement is that the strong suction force of negative pressure slider will affect the accuracy of flying height calibration process.

Considerable work was carried out to confirm the fact that the strong suction force of negative pressure sliders affects the accuracy of calibration process. Both positive pressure slider and negative pressure sliders with and without suspension limiters are included in the analyses. Investigation results show that the calibration error in unloading based calibration is the largest, if the negative pressure slider is mounted on suspension with limiters. The calibration error becomes smaller when using smaller vertical unloading velocity and using shorter light wavelength. A cut-off compensation method is proposed and its feasibility is verified.

Further studies extend to the optical filter. A broader optical filter will cause calibration falloff and therefore affect the accuracy of both calibration and flying height measurement.

This calibration error can be eliminated by using integral response method and the new theoretical curve which are obtained from the integral response method. The new theoretical curve is formed by considering the spectral characteristics of light source, optical filter and photodetector. Experimental results show that the better signal quality and testing accuracy can be achieved by using broader band optical filters.

# Reference

[1] Andreas Moser, Kentaro Takano, David T Margulies, "Magnetic Recording: Advancing Into the Future," *Journal of Applied Physics* Vol. 35, 2002

[2] Bo Liu and Zhimin Yuan, "Tribo-Magnetics and Nanometer Spaced Head-Disk Systems," *IEEE Transactions on Magnetics*, Vol. 37, No. 2, Mar 2001

[3] Yasunaga Mitsuya, Yasuji Ohshima, "Error Analysis of Head-Disk Spacing Measurement Made by Using Optical Interferometry," *ASME J. Tribology*, Vol. 123, April 2001

[4] Klaas B. Klaassen, Jacobus C, "Method and Circuitry For In-Situ Measurement of Transducer/Recording Medium Clearance and Transducer Magnetic Instability," US patent 5,130,866

[5] B. R. Brown, H. L. Hu, K. B. Klaassen, J. J. Lum, J. Van Peppen, W. E. Weresin, "Method and Apparatus for In-Situ Measurement of Head/Recording Medium Clearance," US patent 4,777,544

[6] Zhimin Yuan, Bo Liu, Wei Zhang and Shengbin Hu "Engineering Study of Triple-Harmonic Method for In Situ Characterization of Head-Disk Spacing," *Journal of Magnetism and Magnetic Materials*, Vol. 239, PP 367-370, 2002

[7] Bo Liu and Qisuo Chen, "Carrier Erasure Current Method for In-Situ Monitoring of Head-Disk Spacing Variation" *IEEE Transactions on Magnetics*, Vol. 35, No. 2, Mar 1999

[8] Bo Liu and Zhimin Yuan, "A Scanning Carrier Current method for the In-Situ Monitoring of Head-Disk Spacing," Patent filing

[9] B. Bhushan, *Tribology and Mechanics of Magnetic Storage Devices*, 2nd edition, 1996

[10] C. Lacey, “Method and Apparatus to Calibration Intensity and Determine Fringe Order for Interferometric Measurement of Small Spacings,” US patent, 5,280,340

[11] C. Lacey and E. W. Russ, “Method and Apparatus to Calibration Intensity and Determine Fringe Order for Interferometric Measurement of Small Spacings,” US patent, 5,457,534

[12] P. de Groot, “Optical Gap Measuring Apparatus and Method,” US patent 5,557,399

[13] Carlos A. Duran, “Error Analysis of a Multiwavelength Dynamic Flying Height Tester,” *IEEE Transactions on Magnetics*, Vol. 23, No. 5, Sep 1996

[14] B. Liu and Zhimin Yuan, “In-Situ Characterization of Head-Disk Clearance,” Invited Paper, *ASME/Tribology Division, TRIB*, Vol.10, PP 51-58, Symp, Seattle USA

[15] C. Lin, R. F. Sulliran, “An Application of White Light Interferoemetry in Thin Film Measurement,” IBM, *Journal of Research and development*, California

[16] Yufeng Li, “Flying Height Measurement Metrology for Ultra-Low Spacing in Rigid Magnetic Recording,” *IEEE Transactions on Magnetics*, 32, No.1, Jan 1996

[17] C. Denis Mee and Eric D. Daniel, “Magnetic Recording Technology,” Mc Graw-Hill, 1990

[18] Bo Liu and Zhimin Yuan, “Methodology and Data Pattern for In-Situ Measurement of Head-Disk Spacing,” Patent pending

[19] Corley W. Struck and Paul J. Sides, “Calibration Method for Measurement of Linear Nanometric Distances by Scattered Total Internal Reflection,” *Applied Optics*, Vol. 43, No. 10, April 2004

[20] P. de Groot, L. Deck, J. Soobitsky and J. Biegen, “Optical Flying Height Testing of Magnetic Read-Write Heads,” *Proc. SPIE* 2782, PP 47-57, 1996

[21] R. A. Houston, *Physical Optics*, Blackie & Son Limited, London 1968, PP 49-58

[22] R. W. Wood, *Physical Optics*, The Mac Millan Company, New York 1934, PP 188-194

[23] S. Tolansky, *Multiple-Beam Interferometry of Surfaces and Films*, Oxford University Press, London 1948, PP 161-163

[24] F. A. Jenkins and H. E. White, *Fundamentals of Optics*, McGraw-Hill Book Company, Inc., New York 1957, PP 250-251

[25] M. Francon, *Optical Interfeometry*, Academic press, New York 1996

[26] P. Hariharan, *Optical Interfeometry*, Academic press, Orlando, Florida, 1985

[27] G. Sommargren, "Flying Height and Topography Measuring Interferometer," US patent 5,218,424

[28] P. de Groot, L. Deck, J. Soobitsky, J. Biegen, "Polarization Interferometer for Measuring the Flying Height of Magnetic Read-Write Heads," *Optical letters*, Vol.21, PP 441-443, 1996

[29] Carlos A. Duran, "Flying Height Test Considerations," White Paper

[30] Peng J. P, "Theoretical Prediction of Ramp Loading/Unloading Process in Hard Disk Drives," *ASME J. Tribology*, 121, No.3, 1999, PP 568-574

[31] M. Chapin, D. B. Bogy, "Air Bearing Force Measurement of Pico Negative Pressure Sliders During Dynamic Unload," *J.Tribology*, Vol.122, Oct.2000

[32] Bo Liu and Yufei Han, "Writing Induced Nanodeformation and Its Effects on Head-Disk Clearance," *Journal of Applied Physics*, Vol. 93, No. 10, May 2003

[33] Yong Hu, P. M. Jones, P. T. Chang, "Partial Contact Air Bearing Characteristic of Tripad Sliders for Proximity Recording," *ASME J. Tribology*, Vol. 120, April 1998

[34] Paul M. Chirlian, "Signals and Filters," New York 1994

[35] Q. H. Zeng and D. B. Bogy, "Effects of Suspension Limiters on the Dynamic Load/Unload Process: Numerical Simulation," *IEEE Transactions on Magnetics*, Vol. 35, 1999, PP 2490-2492

[36] Q. H. Zeng, M. Chapin and D. B. Bogy, "Dynamics of the Unload Process for Negative Pressure Sliders," *IEEE Transactions on Magnetics*, 35, No.2, 1998 PP 916-920

[37] M. Chapin and D. B. Bogy, "Air Bearing Force Measurement of Pico Negative Pressure Sliders During Dynamic Unload," *Journal of Triology*, Vol. 122, Oct 2000

[38] Joseph C. Palais, *Fiber optic Communications*, New Jersey